Diagnostic applications of diffuse reflectance spectroscopy

Lise Lyngsnes Randeberg

DOCTORAL THESIS

"First you guess. Don't laugh, this is the most important step. Then you compute the consequences. Compare the consequences to experience. If it disagrees with experience, the guess is wrong. In that simple statement is the key to science. It doesn't matter how beautiful your guess is or how smart you are or what your name is. If it disagrees with experience, it's wrong. That's all there is to it."

Richard Feynman

Preface

The work included in this thesis was carried out at the Department of Electronics and Telecommunications at the Norwegian University of Science and Technology in the period October 1999 – March 2005.

Many people have contributed to make this thesis possible. First of all I wish to thank professor Lars O. Svaasand who has been my supervisor. It has been a pleasure, but also a challenge to work with him. I am very grateful that I was given this opportunity. He is a man with a creative mind, always planning a new experiment, and as a doctoral student you sometimes struggle to keep up. He expects that you make an effort, but if you do, you are always certain to be met with interested questions and plenty of time. Professor Svaasand has made it possible for me to travel a lot, he has introduced me to the scientific community and encouraged me to get my own contacts. Among other things he introduced me at Beckman Laser Institute and Medical Clinic.

I also wish to thank all my co-authors for their cooperation and contributions to my work. My former master students also need to be mentioned, they caused a lot of frustrations and creative solutions. Especially, I wish to thank Arne and Eivind for their help in the lab, and Sandra and Andreas for collecting and systematizing all those data.

This thesis has been a true interdisciplinary work and I have worked with a lot of brilliant people. Just to mention a few: professor Olav A. Haugen who gave us the idea for the optical characterization of bruises. The people at the Department of Dermatology, and especially dr. Jon Helge Bonesrønning and dr. Morten Dalaker for their patience and goodwill with my project. Recently, I have been collecting data at St. Elisabeth Cardiac Center, and I wish to thank the staff and patients for their collaboration. Dr. Rune Haaverstad and Maryann Stenvik must be mentioned for letting me in, and I also want to thank the nurses at St. Elisabeth for their attention and support.

The people at the Department of Electronics and Telecommunications have been good colleagues and friends for the last 5 years. No one of my colleagues should be forgotten. Especially not Joar, without him I would never have continued as a doctoral student after my master degree. He is one of the kindest persons I have ever met. Magnus and I struggled with the diffusion theory together, and luckily we both survived. Magnus is a helpful and intelligent person and it has been a pleasure for me to make his acquaintance. Astrid is not only the female alibi for the department, but also a person I respect for her involvement.

I also have to thank my friends and colleagues in NOFFOF for their support and professional attitude. Lill Tove, Terje and Ellen have been very good friends and colleagues, supporting me via email and phone from Oslo. Without them, this thesis would not have been written. I also wish to thank Odrun for including me in her PDT-research and other activities broadening my mind.

Tekna has been, and will also in the future be a place where I can focus on something completely different. Bjørn and Magnus deserve some special attention. A late night at Studentersamfundet, Bjørn and I decided to do a project together on the mechanical stuff going on in a trauma. Bjørn introduced me to dr. Haaverstad and thereby gave me access to one of my best data sources.

If any of the work included in this thesis results in a patent, it will be due to Magnus. He has been constantly nagging me about patents the last two years. However, he is also a nice guy and good friend.

Finally, I wish to thank my other friends and family for not letting med down during the past years. I haven't been the most sociable person during this period. I especially wish to thank Elin for dragging me away from work to have Camembert and tea with her. The person that have meant most to me is my dear husband Rolf Tore. He never stopped believing in me and my ability to finish this thesis, and fortunately he was right. Without him the layout of all my manuscripts and this thesis probably would have been quite bad. He is the person that introduces some structure and tidiness to my otherwise chaotic life. Our children Ragna, Inga and Sigurd shall all have big hugs for helping me to relax and focus on other things than my research. I would probably have been a poor researcher without their love.

Abstract

This thesis covers a wide field of applications, with an emphasis on applications of reflectance spectroscopy for diagnostic purposes. Reflectance spectroscopy in the visible part of the spectrum has been proved to be a valuable tool in a variety of applications including *e. g.* port-wine stain diagnostics, diagnostics of liver pathology, neonatal jaundice and age determination of bruises for forensic applications.

List of papers

Included papers

The included papers are listed in chronological order. Papers I, II, IV, VI, VII consider various aspects of port-wine stain diagnosis, treatment or treatment monitoring. Paper III considers the use of reflectance spectroscopy as a tool for optical diagnosis of pathological liver changes. Paper VIII considers optical detection of bilirubin levels in neonatal jaundice, and the use of spectroscopy to monitor physiological changes during light therapy of neonatal jaundice. Papers V and IX consider optical characterization of bruises in forensic medicine.

I: L.L. Randeberg, L.O. Svaasand, Simulated color: a diagnostic tool for skin lesions like port-wine stain, Proceedings of SPIE, 4244:1 – 12, 2001

II: L.L. Randeberg, A.J. Daae Hagen, L.O. Svaasand, Optical properties of human blood as a function of temperature, Proceedings of SPIE, 4609:20 – 28, 2002

III: L.L. Randeberg, O.A. Haugen, L.O. Svaasand, Optical diagnostics of liver pathology, Proceedings of SPIE, 5141:187 – 195, 2003

IV: L.O. Svaasand, L.L. Randeberg, G. Agiular, B. Majaron, S. Kimel, E.J. Lavernia, J.S. Nelson, Cooling efficiency of cryogen spray during laser therapy of skin, Lasers Surg Med, 32(2):137 – 142, 2003

V: L.L. Randeberg, A. Winnem, S. Blindheim, O.A. Haugen, L.O. Svaasand, Optical classification of bruises, Proceedings of SPIE, 5312:54 – 64, 2004

VI: L.L. Randeberg, J.H. Bonesrønning, M. Dalaker, J.S. Nelson, L.O. Svaasand, Methemoglobin formation during laser induced photothermolysis of vascular skin lesions, Lasers Surg Med, 34(5):414 – 419, 2004

VII: L.O. Svaasand, G. Aguilar, J.A. Viator, L.L. Randeberg, S. Kimel, J.S. Nelson, Increase of dermal blood volume fraction reduces the threshold for laser-induced purpura: Implications for port wine stain laser treatment, Lasers Surg Med, 34(2):182 – 188, 2004

VIII: L.L. Randeberg, E.B. Roll, L.T. Norvang Nilsen, T. Christensen, L.O. Svaasand, *In vivo* spectroscopy of newborn skin reveals more than a bilirubin index, Acta Paediatrica, 94(1):65 – 71, 2005

IX: L.L. Randeberg, O.A. Haugen, R. Haaverstad, L.O. Svaasand, Age determination of traumatic injuries, Submitted to Lasers Surg Med, March 2005

My contributions

All papers were written under the influence of professor Lars O. Svaasand's ideas. Although his direct contributions are not listed for some of the papers, he has been a source of inspiration and a discussion partner during the data analysis and writing of all the papers. The papers cover a wide range of topics and are the result of interdisciplinary cooperation. Interdisciplinary work is a challenge, and most of my work has been totally dependent on goodwill from the medical staff at St. Olav's hospital. I felt a strong obligation to not interfere with their daily work, and therefore it has been difficult to do follow-up studies so far. The importance of follow-up studies is obvious and there will be put in a large effort to initiate further work in at least some of the areas presented in this thesis. My contributions to each of the included papers are given below.

I: The paper was based on experimental data from Lill Tove Norvang Nilsen. I developed the model, tested it and wrote the manuscript. The model was based on CIE-standards for calculation and transformation of color coordinates. It was tested on experimental data and data simulated using the optical transport model developed by Svaasand, Norvang and Spott.

II: I wrote the paper based on experimental work carried out in cooperation with Arne Johan Daae Hagen during his diploma work. I did all absorption spectroscopy and data analysis, whereas the fluence rate measurements were carried out by Hagen.

III: The measurements were carried out in the department of pathology on tissue samples collected by professor Olav A. Haugen. He did the histology and the analysis of the histology data. I did the spectroscopic measurements, all other data analysis and wrote the paper.

IV: This paper was written by professor Svaasand. I were engaged in the production of the sensor, collected the experimental data, and carried out the direct analysis of the data based on professor Svaasand's theory. I produced some of the figures included in the paper and proofread the manuscript.

V: This work was carried out in connection with the 5th year project works of Sandra Blindheim and Andreas Meyer Winnem. I supervised their project works and their diplomas, did most of the data analysis and wrote the manuscript. The experimental data were collected by Blindheim, and organized and partly analyzed by Winnem.

VI: This work was carried out at the Dept. of Dermatology in cooperation with dr. Jon Helge Bonesrønning and dr. Morten Dalaker. They recruited the patients, and I carried out the measurements, did all data analysis, and wrote the manuscript.

VII: This paper was written by professor Svaasand. I contributed to the work by carrying out the initial reflectance measurements to check the effect of vacuum on the blood volume in the skin.

VIII: This paper was based on experimental data collected by Peter Schmedling during his diploma thesis in 1996. His thesis was supervised by Ellen Bruzell, Lill Tove Norvang Nilsen, Lars O. Svaasand and Terje Christensen. All data analysis was carried out by me. Ellen Bruzell did the medical analysis of the results and their impact. The manuscript was written by me with contributions from Bruzell on the medical background and analysis.

IX: This paper was written by me based on experiments carried out at St. Elisabeth Cardiac Center. These measurements were made possible by dr. Rune Haaverstad and carried out under his supervision of the recruitment of patients. All measurements and data analysis were carried out by me. Professor Svaasand contributed to the writing of the manuscript and to the mathematical modelling.

Other published work

Relevant work not included in the thesis is listed below.

1. L.L. Randeberg, R. Haaverstad, R. Wiseth, A.M. Winnem, O.A. Haugen, L.O. Svaasand, Optical characterization of skin hematomas, ASLMS 25th Annual meeting, Orlando, March 30 – April 3, 2005, Lasers Surg Med, 36(Suppl 17):p16, 2005

2. M.B. Lilledahl, O.A. Haugen, L.L. Randeberg, L.O. Svaasand, Optical characterization of artherosclerotic plaque by reflection spectroscopy, Accepted: Proceeding of SPIE, Vol. 5686, 2005

3. L.L. Randeberg, J.H. Bonesrønning, M. Dalaker, L.O. Svaasand, Reflectance spectroscopy as a dosimetric tool during laser treatment of vascular lesions, Lasers Med Sci, 18 (Suppl 1):S47 – S48, 2003

4. B. Majaron, G. Aguilar, B. Basinger, L.L. Randeberg, L.O. Svaasand, E.J. Lavernia, J.S. Nelson, Sequential cryogen spraying for heat flux control at the skin surface, Proceedings of SPIE, 4244:74 – 81, 2001

5. L.L. Randeberg, E.B. Roll, L.T. Norvang Nilsen, T. Christensen, L.O. Svaasand, Estimation of bilirubin levels during neonatal jaundice, ESP 2001, 9th Congress of the European Society of Photobiology, Lillehammer, Norway, Sept. 3 – 9, 2001

6. L.L. Randeberg, A.J. Daae Hagen, L.O. Svaasand, Optical properties of human blood as a function of temperature, ICPS 2001, 16th International Conference of Physics Students, Dublin, Ireland, Aug. 10 – 15, 2001

7. L.L. Randeberg, E.B. Roll, L.T. Norvang Nilsen, P.F. Schmedling, L.O. Svaasand, Optical measurement of bilirubin during neonatal jaundice, ASLMS 21th Annual meeting, New Orleans, April 18 – 22, 2001, Lasers Surg Med, 28 (Suppl 13):p6, 2001

8. L.L. Randeberg, L.T. Norvang, P. Helsing, N-J. Mørk, T. Spott, L.O. Svaasand: Visualization in diagnostics and treatment monitoring of physical conditions like port-wine stain, ASLMS 20th Annual Meeting, Reno, April 7 – 9, 2000, Lasers Surg Med, 26 (Suppl 12):p53, 2000

Contents

Chapter 1

Introduction

BIOMEDICAL optics is often considered as a new scientific field, although optical diagnosis has a long history in medicine. Visual examination has been a tool for physicians since ancient times, and is still important in a clinical situation. However, the need for more objective and quantitative methods to support the diagnosis has eventually reached the medical community, and new optical imaging and spectroscopic techniques are developed as an answer to that demand. Optical techniques can provide non-invasive, low cost methods for a variety of applications. Techniques like optical coherence tomography (OCT) and fluorescence imaging have become important techniques for imaging of the retina and cancer diagnostics, respectively. Reflectance spectroscopy is a well known, easy manageable technique to get information about optical properties in tissue. Reflectance spectroscopy is as indicated by the name a spectroscopic technique, limited by the penetration depth into the sample. The penetration depth is the depth where the incident light intensity has been reduced with a factor $1/e$. In human tissue the penetration depth varies with wavelength from a few micrometers in the ultraviolet part of the spectrum to several millimeters in the near infra red. Reflectance spectroscopy as a diagnostic technique is therefore usually applied to conditions affecting the surface or surface near structures. Neonatal jaundice and port-wine stain diagnostics are examples of conditions where reflectance spectroscopy has been utilized successfully [1, 2]. The choice of diagnostic technique depends on the application. Deep structures are often diagnosed using imaging techniques like CT or MR, exhibiting a large penetration and good spatial resolution. Temporal resolution and velocity imaging can be achieved using ultrasound or optically based techniques like doppler OCT or laser doppler.

This thesis focus on diagnostic applications of reflectance spectroscopy. The main aim of the thesis was to develop new diagnostic techniques based on well known spectroscopic techniques. The thesis is based on nine papers that have been organized into three main parts considering port-wine stain diagnostics and treatment, optical properties of tissue, and forensic applications of reflectance spectroscopy. In the first part of the thesis the emphasis is put on understanding and describing the physical and biologic response to laser exposure and cryogen spray cooling of the skin. Laser treatment of port-wine stains is considered as an established technique, although only about 25 % of the patients experience complete fading of their lesions [3, 4]. Poor therapeutic results in some patients have encouraged development of new techniques like cryogen spray cooling [5]. By cooling the skin surface, a larger light dose can be applied without inducing thermal damage to tissue above the optical target. Another approach to improve therapeutic outcome is to consider optical changes induced by the treatment. In this thesis the thermal effect of slow heating

of blood has been investigated, and formation of methemoglobin was revealed. This finding was consistent with previously reported results [6, 7, 8]. The *in vitro* experiments were followed by *in vivo* detection of methemoglobin formation induced by laser exposure.

The second part of the thesis includes detection of liver pathology by the use of reflectance spectroscopy, and detection of bilirubin and light induced changes in neonatal jaundice.

The third part of the thesis considers optical diagnostics of skin hematomas, for use in forensic medicine. Bruises exhibit visible color changes well suited for spectroscopy. In legal medicine it is important to have objective, quantitative methods. The task of determining the age of an injury is an example of an area where objective methods would be valuable. The yellow color in old bruises is caused by bilirubin, and spectroscopic detection of bilirubin is a well known technique from neonatal jaundice diagnosis [2, 9, 10]. Spectroscopic detection of bilirubin in bruises has been suggested as a tool for age determination of bruises [11]. However, work carried out in this thesis indicate that bilirubin cannot be used as the only marker to determine the age of skin contusions. A mathematical model has been developed to describe the temporal development of subcutaneous bruises. The presented model is based on diffusion theory, and takes both hemoglobin and bilirubin into account in the age determination process. The model still needs refinement, but have in preliminary results proved to date bruises with an accuracy of approximately one day. The presented method is a very first approach to combine diffusion theory and reflectance spectroscopy to date bruises.

Chapter 2

Tissue optics

"Sucking on the skin makes it red."

R. Rox Anderson

OPTICAL diagnostics of human skin is an important part of this thesis. To be able to understand and interpret the experimental data and construct theoretical models it is essential to have knowledge about skin optics and physiology. This chapter is therefore included to summarize the optical and physical properties of human skin.

2.1   Skin physiology

Skin is a layered structure designed to protect the human organism against environmental stress such as infections, excess amounts of optical radiation, dehydration or heat. The skin is divided into three main layers; epidermis, dermis and the subcutis. The upper skin layer, epidermis, is typically $50 - 80 \, \mu$m thick, and can be subdivided into another five layers. From the surface these layers are stratum corneum, stratum lucidum, stratum granulosum, stratum spinosum and stratum basale [12]. A sketch of human skin is shown in Fig. 2.1. In this thesis the epidermis is considered as one layer incorporating the joint optical properties of all epidermal layers, including the vascular system of the basal layer, the outer boundary of the stratum corneum, and the pigmentation.

The pigment, melanin, is produced by melanocytes, usually found in the basal layer. Melanin is released in vesicles called melanosomes and transported via dendrites to adjacent keratinocytes [14, 15]. Human skin color is strongly influenced by pigmentation, and the amount, shape and size of melanosomes within the epidermis is genetically determined. Caucasian melanosomes typically contain a larger amount of melanin granules, but less total melanin than Negroid or Mongolian melanosomes [15]. Caucasian melanosomes have a long axis of approximately 400 nm, and tend to occur in clusters of three to eight. Negroid melanosomes are larger with a long axis of approximately 800 nm and do not tend to cluster. The melanosome density in the skin varies with body site, with the highest density in areas exposed to sun. However, the melanosome density does not vary with race [14]. The optical properties of melanin is further described below.

Skin can be classified due to pigmentation using the Fitzpatrick scale from skin type I to VI [16]. Using this scale, Caucasian individuals with Scandinavian heritage usually have skin type I,
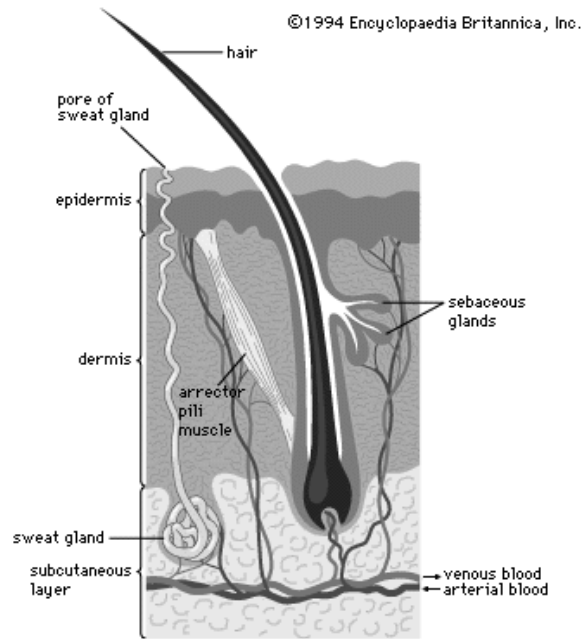
Figure 2.1: Cross section of human skin. Figure from Encyclopaedia Britannica Online [13].

II or III. A darkening of the skin color occurs after UV exposure, and at least two mechanisms are active in this respect. UVA radiation induces immediate pigment darkening, whereas UVB gives a delayed pigment darkening $2-3$ days after exposure [14, 17, 18]. Details in the mechanisms of pigment darkening, induction of erythema following UV exposure and photo protection processes are still unknown.

The dermis is thicker than the epidermis, usually $1-4$ mm, and has a more complex structure including hair follicles, sweat glands, sensory nerve systems, blood vessels and connective tissue [12]. The skin thickness varies with body site, age, gender and smoking habits [19]. The connective tissue gives support and elastic strength to the skin. The vascular system of the dermis is divided into the upper and lower vasculary plexus, connected by vertical supply vessels. Below the dermis the subcutaneous fatty layer provides insulation and protection against mechanical injury [12].

2.2   Absorption and scattering

When photons hit biological tissue they can be reflected, absorbed, scattered or transmitted, depending on the wavelength and the optical properties of the sample. Thus, the shapes of reflectance and absorption spectra are dependent on light absorbing and scattering substances within the sample, *i. e.* the chemical composition of the sample. The spectral features of a chromophore can be described mathematically using absorption and scattering cross sections of the chromophore particles. The absorption and scattering cross sections for individual particles can be derived from Maxwell's equations, which describe the interaction between an incident electric field and the particle [20]. The scattering cross section, σ_s describes the ability of a particle to scatter incident electric fields, and the absorption cross section, σ_a describes the total power absorbed by the particle. The total cross section of the particle is given by the sum of the scattering and absorption cross

sections, $\sigma_t = \sigma_s + \sigma_a$. These quantities are related to the absorption and scattering coefficients by the volume density of particles, ρ.

The absorption in a homogeneous, non-scattering medium can be expressed by the use of the Lambert-Beer law

$$I(x) = I(0)e^{-\mu_a x} \tag{2.1}$$

where $I(0)$ is the incident intensity, and μ_a is the absorption coefficient of the medium. Absorption is caused by resonant interactions between molecules and the incident light. Photons interact with molecules in their path, and if the energy of the photons is resonant with the energy levels in molecules, a photon may be absorbed and cause an exited energy state in the absorbing molecule. The transitions in the molecule may be electronic or vibrational transitions depending on the photon energy.

Scattering occurs when incident electric fields are deflected due to a change in refractive index. Scattering is strongly dependent on the size of the scatterer. Rayleigh scattering occurs if the scattering particle is smaller than the wavelength. The scattered field is identical to the scattered field from a dipole. The scattering cross section is in this case proportional to the square of the size of the scatterer and inversely proportional to the fourth power of the wavelength. Sub-cellular biological structures like mitochondria are Rayleigh scatterers. The blue color of the sky is caused by Rayleigh scattering from air molecules. If the size of the particle is larger than the wavelength, the scattering can be described by Mie theory. In Mie theory the electric and magnetics fields within the particle must be considered. The Mie scattering cross section is inversely dependent on the square of the particle radius, and depends weakly on the wavelength. Mie scattering is strongly forward directed. Scattering by fat droplets in milk and scattering by water droplets in clouds are typical examples of Mie scattering. The total attenuation coefficient gives the combined effect of the scattering and absorption in a medium, and is given as $\mu_t = \mu_s + \mu_a$

In the case of multiple scattering it is useful to know the angular distribution of the scattering events. Each time light is scattered it will change direction and move in the new direction until it once more is scattered. Depending on the amount of scattering particles and their scattering efficiency, the photon will travel a given distance between the scattering events. This distance is called the scattering mean free path l_s and is given by the scattering coefficient as $l_s = 1/\mu_s$. The angular distribution of the scattering angles can be described by the anisotropy factor, *i. e.* the average cosine of the scattering angle

$$g = \overline{\cos\theta} \tag{2.2}$$

where θ is the scattering angle. Scattering in skin is strongly forward directed, and the value of g is approximately 0.8. The wavelength dependence of g has been experimentally determined [21] and can be written as:

$$g = 0.62 + 29 \cdot 10^{-5} \cdot \lambda \tag{2.3}$$

where λ is the wavelength in nm. The depth where the photons have lost all information about their incident direction is called the reduced scattering mean free path, and is given by

$$l_s' = \frac{l_s}{1-g} \tag{2.4}$$
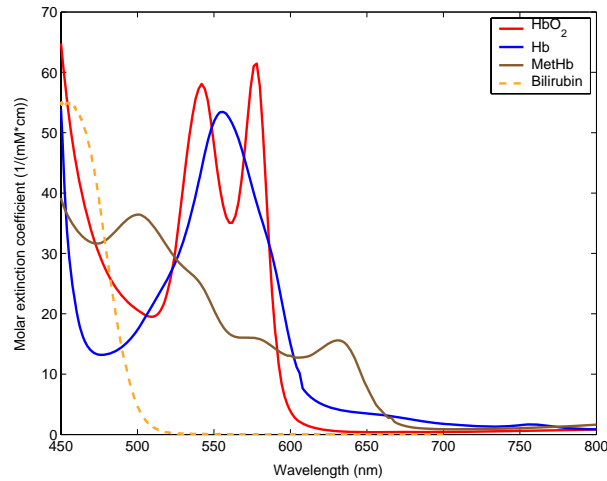
Figure 2.2: Extinction coefficients for hemoglobin, methemoglobin and bilirubin. Data from Zijlstra et al. [25], Du et al. [26].

The reduced scattering coefficient μ_s' is thus defined as

$$\mu_s' = \frac{1}{l_s'} \tag{2.5}$$

The transport coefficient, which describes the effective total attenuation, is then defined in the same manner as the total attenuation coefficient $\mu_{tr} = \mu_s' + \mu_a$.

2.3 Skin optical properties

Knowledge about skin optical properties is essential to reveal information from measured reflectance spectra. Skin contains light absorbing chromophores like melanin, hemoglobin, betacarotene and bilirubin [15].The visual appearance of skin is attributed to both scattering and absorption properties. Tissue scattering is caused by *e. g.* lipids, water and proteins like collagen, and can be described by a combination of Rayleigh and Mie scattering [15, 22, 23, 24].

2.3.1 Blood

The absorption characteristics of blood are mainly due to hemoglobin absorption. Hemoglobin is designed to transport oxygen from the lungs to the extra vascular tissues throughout the body, and return CO_2 back to the lungs. The oxygen binding capacity of the hemoglobin molecules is due to the four heme groups found within each hemoglobin molecule. Heme consists of a porphyrine ring with a central iron atom in the 2+ oxidation state. Hemoglobin without bound oxygen, deoxyhemoglobin (Hb), has a dark red, bluish livid color, while hemoglobin with bound oxygen, oxyhemoglobin (HbO_2), shows a bright red color [15, 25]. Deoxyhemoglobin exhibits absorption maxima at 550 nm and 760 nm, and oxyhemoglobin shows maxima at 548 nm and 576 nm, see Fig. 2.2. If hemoglobin is exposed to oxidative stress, *e. g.* by heating, the iron atom in the heme group can be oxidized to the Fe 3+ state, forming methemoglobin. Methemoglobin is chocolate brown in color and have no ability to carry oxygen [25]. Methemoglobinemia is seen

after overdoses of some drugs or poisoning [27, 28]. Formation of methemoglobin has also been observed by Kollias et al. [8] following exposure to UVB radiation. In this case the UV-light is thought to cause formation of free radicals, and thus oxidative stress. Methemoglobin is formed from HbO_2 in the oxidative reaction [28]

$$Hb(Fe^{2+}) \cdot O_2 \Rightarrow Hb(Fe^{3+}) + O_2^- \tag{2.6}$$

Methemoglobin has characteristic peaks at 404, 508 and 635 nm [8]. Following formation of methemoglobin a decrease in the oxyhemoglobin absorption peaks at 335 nm, 415 nm, 542 nm and 576 nm will occur, as observed by Baranov et al. [29]. Formation of methemoglobin following heat exposure has been reported by several authors [6, 30, 31, 32, 33]. The absorption spectrum of methemoglobin is shown in Fig. 2.2.

The scattering cross section, the absorption cross section, and the anisotropy factor for human erythrocytes are given by Ishimaru [20]. At 685 nm wavelength the value of the scattering cross section, the absorption cross section and the anisotropy factor are $\sigma_{s,b} = 55.09 \cdot 10^{-12}$ m^2, $\sigma_{a,b} = 0.059 \cdot 10^{-12}$ m^2 and $g_b = 0.9949$, respectively. The corresponding values for the absorption and scattering coefficients of whole blood with hematocrit H is then given by [34]

$$
\begin{aligned}
\mu_{a,b} &= \sigma_{a,b} \frac{H}{v_e} \\
\mu_{s,b} &= \sigma_{s,b} \frac{H(1-H)(1.4-H)}{v_e} \\
\mu'_{s,b} &= \sigma_{s,b} \frac{H(1-H)(1.4-H)}{v_e}(1-g_b)
\end{aligned}
\tag{2.7}
$$

where the volume of the erythrocytes is assumed to be $v_e = 1.25 \cdot 10^{-16}$ m^3, and where $\mu_{a,b}$, $\mu_{s,b}$ and $\mu'_{s,b}$ are the absorption coefficient, the scattering coefficient and the reduced scattering coefficient, respectively. The hematocrit value $H = 0.41$ is used for adult subjects. This value is within the range of the normal values for both male and female adults [35]. Infants have hematocrit values in the range $H = 0.45-0.65$ with a mean value $H = 0.55$ [36]. The wavelength dependency of the scattering coefficient can be approximated by Mie theory [24], and this wavelength dependence is proportional to $\lambda^{-0.37}$ [37]. Thus, the reduced scattering coefficient, $\mu''_{s,b}$, can be expressed [38]

$$\mu''_{s,b} = \sigma_{s,b} \frac{H(1-H)(1.4-H)}{v_e}(1-g_b)\left(\frac{685\text{nm}}{\lambda}\right)^{0.37} \tag{2.8}$$

The wavelength dependence of the absorption coefficient is given in Fig. 2.2. The absorption coefficient of hemoglobin depends strongly on the oxygenation. The oxygenation can be determined from the ratio of the blood absorption at an isosbestic point and a nonisosbestic point [20]. The equation given by Ishimaru was modified by Spott et al. [38] to calculate the oxygenation from the dermal absorption coefficient:

$$OS = \frac{\mu_{Hb}(\lambda_1) - \mu_{Hb}(\lambda_2) \cdot \frac{\mu_a(\lambda_1)}{\mu_a(\lambda_2)}}{\mu_{Hb}(\lambda_1) - \mu_{HbO_2}(\lambda_1)} \tag{2.9}$$

where OS is the oxygen saturation in percent, μ_a is the measured absorption coefficient, and μ_{Hb} and μ_{HbO_2} are the specific absorption coefficients of deoxygenated and oxygenated blood, respectively [25]. The wavelengths λ_1 and λ_2 are a nonisosbestic and an isosbestic point, respectively. The oxygenation depends on the wavelengths chosen for the calculations, due to the variation in oxygenation with skin depth. The calculated oxygenation value at a certain wavelength correspond to the penetration depth in that specific spectral range [39].

2.3.2   Melanin

Melanin is a protein-polymer complex found within melanosomes in the epidermis [15]. Two kinds of melanin; alkali soluble, red-yellow phaeomelanin, and insoluble, black-brown eumelanin can be found in human skin. The individual hair and skin color is determined by the total melanin content and the ratio between the two melanin spices [14, 18]. Melanin has a broad absorption band ranging from the ultra violet into the near infrared parts of the spectrum [18]. The apparent skin color and thus the skin reflectance depends on the melanin content within the skin. The melanin absorption decreases with increasing wavelength proportional to $\lambda^{-3.46}$ [23]. Thus can the melanin absorption be described by [1, 40]

$$\mu_{a,m} = 225\,\mathrm{m}^{-1} \left(\frac{694\,\mathrm{nm}}{\lambda} \right)^{3.46} \tag{2.10}$$

where the value of the melanin absorption coefficient was found to be $\mu_{a,m} = 225$ m^{-1} at 694 nm for fair, sun protected Caucasian skin.

2.3.3   Bilirubin

Bilirubin exhibits a characteristic absorption peak at 460 nm, giving the compound a yellow/orange color [15, 26]. The bilirubin absorption within skin can be observed in reflectance spectra in the wavelength range $450-480$ nm [39]. The absorption spectrum of bilirubin dissolved in chloroform is shown in Fig. 2.2.

Bilirubin is formed during breakdown of heme containing proteins, such as hemoglobin and myoglobin [41, 42]. Hemoglobin breakdown occurs mainly in the liver, and is dependent on the heme oxygenase system [42, 43]. In newborns the bilirubin production is elevated due to a high hemoglobin turnover after birth. Bilirubin accumulation in skin causes a characteristic yellow skin color. This condition is called hyperbilirubinemia or jaundice. As many as 50 % of all newborns suffer from some degree of hyperbilirubinemia, due to low enzyme activity in the liver. Bilirubin is toxic and high concentrations can cause brain damage, hence $5-10$ % of all newborns receive therapy for jaundice. This treatment might be light therapy or blood transfusion in severe cases [41, 44].

Bilirubin is also the chromophore responsible for the yellow color observed in old bruises. This connection was found by Virchow [45] as early as 1847. In the case of bruised skin the hemoglobin is broken down by macrophages recruited to the injured area by chemical signals released following local trauma. Macrophages phagocytize both whole erythrocytes and hemoglobin molecules and catabolize the hemoglobin using the heme oxygenase system [46, 47, 48, 49]. A overview of the hemoglobin breakdown occurring within bruised skin is given in Fig. 2.3. After the globin moiety of hemoglobin has been removed, the closed ring structure of heme is broken
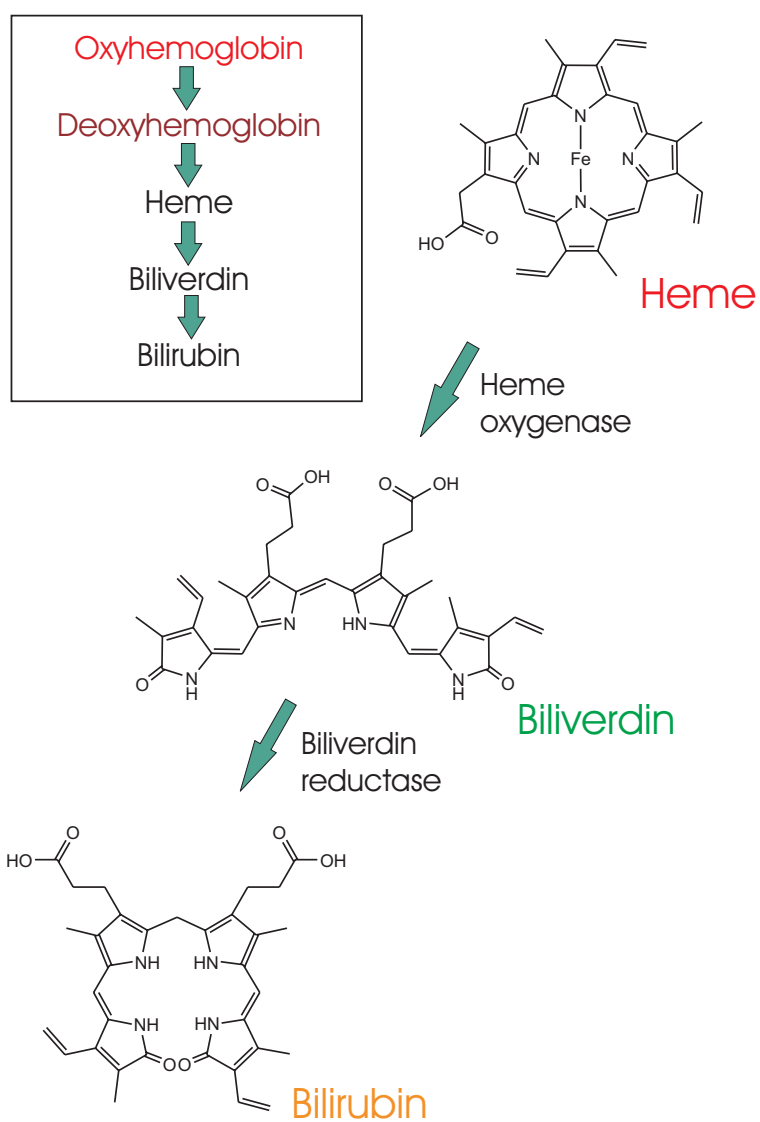
Figure 2.3: Chemcial breakdown of hemoglobin. Structure formulas from CambridgeSoft [50].

by heme oxygenase and the tetrapyrrole biliverdin is formed [42]. Biliverdin is, as indicated by its name, a green pigment. In human skin heme oxygenase is the rate limiting enzyme, and biliverdin is a short lived chromophore due to the high biliverdin reductase activity. Bilirubin is removed slowly from the injured site by *e. g.* the lymphatic system. Hemosiderin is a brown chromophore produced from heme breakdown products within the macrophages. Hemosiderin might be found within resident tissue macrophages for months after a trauma [11, 46, 47, 48, 49].

2.3.4 Background tissue absorption

Scattering is the dominating optical process in normal dermis. The scattering is caused *e. g.* by differences in the index of refraction between the collagen fibers and the surrounding tissue. The scattering properties are important for the appearance of the skin and the skin color. The scattering properties of the epidermis resembles the properties of the dermis. The scattering in infant skin has been described by Saidi et al. [22] using Rayleigh and Mie theory. The reduced scattering coefficient $\mu'_{s,tissue}$ was found to be dependent on the gestational age and can be given by

$$\mu'_{s,tissue} = C_{Mie} \left(1 - 1.745 \cdot 10^{-3}\lambda + 9.8443 \cdot 10^{-7}\lambda^2\right) + C_{Rayleigh}\lambda^{-4} \qquad (2.11)$$

where C_{Mie} is the Mie constant, and $C_{Rayleigh}$ is the Rayleigh constant. For a gestational age of 39 weeks the Mie constant is $C_{Mie} = 6800$ m^{-1}, for the same gestational age the Rayleigh constant is, $C_{Rayleigh} = 9.5 \cdot 10^{13}$ nm^4/m. The wavelength λ is given in nm. Svaasand et al. [1] used the value $\mu_s = 50$ mm^{-1} for $\lambda = 577$ nm for the scattering coefficient [51, 52]. The reported values vary substantially and measurements indicate a lower value [21].

Background absorption in tissue is caused by other factors than hemoglobin, methemoglobin, bilirubin, betacarotene or melanin and is assumed to be comparable to the absorption seen in ocular tissue, $\mu_n = 25$ m^{-1} [1, 53]. The value of μ_n is applied to both epidermis and dermis.

2.3.5 Other absorbers

Carotenoids such as betacarotene are found in low concentrations in skin. Carotenoids are yellow to red lipofilic pigments found in fruits and vegetables. Betacarotene has a characteristic absorption with a double peak at 450 and 480 nm [26, 54]. Carotenoids are accumulated in skin after consumption of fruit and vegetables and are believed to have some beneficial effects due to their capability to scavenge free radicals. Betacarotene accumulates in the subcutaneous fatty tissue and the stratum corneum, giving a distinct yellow color, specially in regions like the palm of the hand and the sole of the foot where the stratum corneum is more pronounced [26, 55, 56].

Water absorption is low in the visible region of the spectrum. Water absorption increases for wavelengths above 600 nm, and shows an absorption minimum at 418 nm [57]. The absorption coefficient for water is shown in Fig. 2.4.

Other chromophores are pyrines and pyrimidines found in nucleic acids. These chromophores mainly absorb light with wavelengths shorter than 300 nm, and are thus not of importance in this work. Other chromophores like riboflavin and porphyrines absorb light in the UV and visible part of the spectrum, but are only found in small amounts in normal skin. Hence, they are not included in the models used in this work [15, 26].
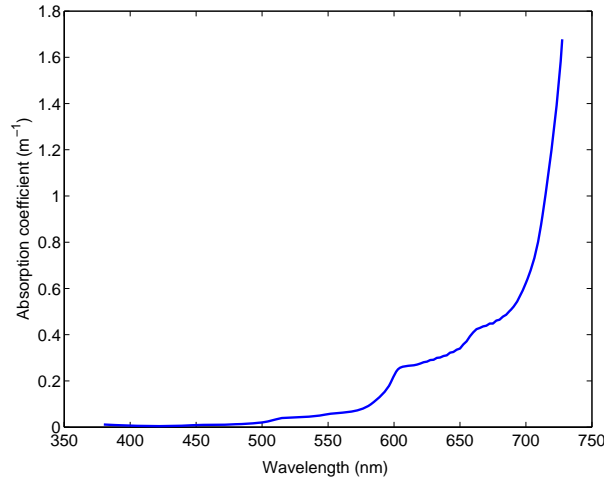
Figure 2.4: Absorption coefficient for water. Data from Pope and Fry [57].

2.3.6 Total absorption and scattering coefficients in human skin

In the present models for light propagation in tissue, see Ch. 4, the total absorption and scattering coefficients, $\mu_{s,e}, \mu_{s,d}, \mu_{a,e}$ and $\mu_{a,d}$ for epidermis and dermis are given by

$$\mu_{a,e} = \mu_{a,b}B_e + (\mu_{a,m} + \mu_n)(1 - B_e) \tag{2.12}$$

$$\mu'_{s,e} = \mu'_{s,\text{tissue}}(1 - B_e) + \mu''_{s,b}B_e \tag{2.13}$$

$$\mu_{a,d} = \mu_{a,b}B_d + \mu_{a,br}B_{br} + \mu_{a,met}B_{met} + \mu_{a,beta}B_{beta} + \mu_n(1 - B_d) \tag{2.14}$$

$$\mu'_{s,d} = \mu'_{s,\text{tissue}}(1 - B_d) + \mu''_{s,b}B_d \tag{2.15}$$

where B_e and B_d are the blood volume fraction in epidermis and dermis, respectively. This model is an extended version of earlier models [1, 38] The absorption coefficient in dermis, $\mu_{a,d}$, is a combination of the blood absorption $\mu_{a,b}$, the background absorption μ_n, and the absorption in bilirubin $\mu_{a,br}$, methemoglobin $\mu_{a,met}$ and betacarotene $\mu_{a,beta}$. The absorption in bilirubin, betacarotene and methemoglobin is scaled according to their volume fractions in dermis, B_{br}, B_{met} and B_{beta}.

If a hemorrhage is to be modeled, an additional blood absorption is added as a separate variable. The blood absorption in the injury may be different from the background blood absorption with respect to oxygenation and blood volume fraction.

Chapter 3

Experimental techniques

"The pure and simple truth is rarely pure and never simple."

Oscar Wilde

THE art of experimental work is difficult, challenging, and filled with hidden treasures. This chapter was included to focus on the limitations of experimental work. There is no such thing as a perfect experiment, the results are always perturbed by the measurement. The challenge for an experimentalist is to minimize the perturbation and to be able to differentiate a real discovery and a lousy experiment. One of the greatest challenges in biomedical optics is the unpredictable behavior of the samples. Individual differences in *e. g.* blood flow, hydration and pigmentation must be taken care of and corrected for to be able to compare results from different samples. Most of the scientists working in this field know this, and struggle with such problems regularly. However, artifacts due to technical equipment is often ignored or underestimated. Such artifacts may be avoided by considering the impact of technical specifications on the experiments.

In this chapter I have chosen to focus on absorption and reflectance spectroscopy since these techniques are the most important techniques used in my work. Other experimental techniques are described in the respective papers. A brief discussion of variability of the samples is also included. All technical information presented in this chapter was found at the suppliers' web sites:

– www.agilent.com/chem/

– www.ocean.optics.com

– www.labsphere.com

3.1   Absorption spectroscopy

The absorption spectroscopy in paper II was carried out using a diode array spectrometer (HP8453, Hewlett-Packard GmbH, Waldbronn, Germany). This spectrometer has a wavelength range $190 - 1100$ nm, and is equipped with two light sources to cover the entire range. The light sources are a halogen lamp and a deuterium lamp assuring a good signal to noise ratio even in the ultra violet part of the spectrum. The wavelength accuracy is better than $\pm\, 0.5$ nm and the wavelength
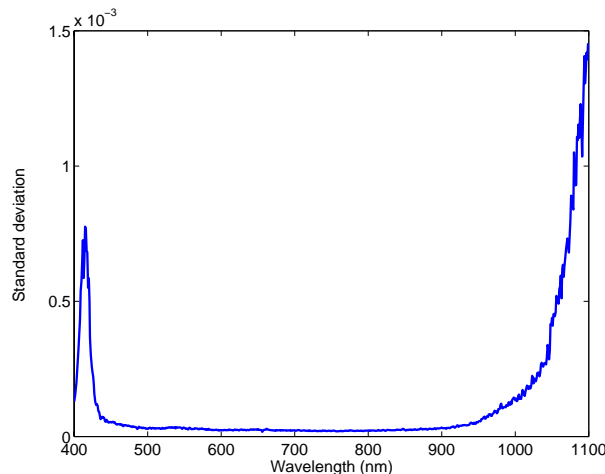
Figure 3.1: Typical standard deviation in hemoglobin absorption measurements on HP8453 diode array spectrometer.

reproducibility is better than $\pm$ 0.02 nm in ten consecutive scans. A typical scanning time is 1.5 s with 0.5 s integration time. All the measurements presented in paper II were collected using an integration time of 10 s. The warm up time for the equipment was one hour.

The absorption measurements were carried out using disposable plastic cuvettes. These cuvettes may have limited the transmission through the samples for wavelengths in the ultra violet, however this was not considered as a problem since the focus was on the wavelength range 400 – 850 nm. The plastic cuvettes were chosen instead of quartz cuvettes to limit the amount of cleaning. The measurements were done on human blood and it was desirable to avoid unnecessary handling of equipment contaminated with blood.

The measurements were calibrated using a cuvette filled with distilled water, and all air bubbles observed inside the cuvettes were removed prior to measurement. The instrument drifted substantially, and had to be re-calibrated frequently. The drift was visible even within one measurement series, causing negative absorption values in some of the samples. The absorbance data in the study were normalized at given wavelengths, *e. g.* 3.0 at 576 nm or 1.5 at 585 nm. This was done to avoid the concentration error introduced when diluting the samples. The calibration wavelengths were chosen to visualize the spectral changes with respect to the oxyhemoglobin content in the samples. Sedimentation was seen within the samples waiting in line for measurement, and this effect was removed by capping the cuvettes and turning them slowly upside down before measurement.

The reproducibility of these measurements was good when the re-calibration was carried out frequently. All measurements were repeated three times to cancel out statistical variations. Typical standard deviation for hemoglobin absorption measurements is shown in Fig. 3.1. The peak seen in the standard deviation at approximately 400 nm is probably caused by the high absorbance values measured in the hemoglobin samples in this wavelength range. The increasing standard deviation for wavelengths longer than approximately 900 nm is probably due to the silicon detector. The band gap wavelength in silicon is found at approximately 1100 nm, and the performance of the detector decreases close to this wavelength.
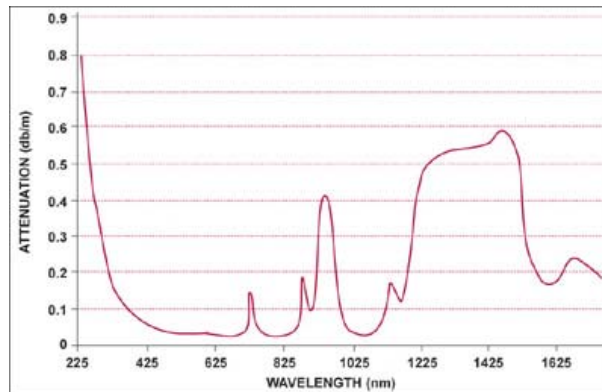
Figure 3.2: Transmission characteristics of an Ocean Optics UV/VIS multi mode optical fiber.

3.2 Reflection spectroscopy

The reflectance measurements were collected using two different spectrometers. The results presented in papers I and VIII, were measured with the Hewlett Packard diode array spectrometer described above, equipped with a reflectance accessory (RSA-HP-53, Labsphere, North Sutton, NH, USA). The reflectance data in paper VII were measured using an earlier version of the Hewlett Packard spectrometer (Hewlett Packard 8452A, Labsphere RSA-HP-84 reflectance accessory). This spectrometer has a shorter wavelength range, and lower wavelength resolution. However, it is regarded as comparable to the HP 8453. The spectra presented in papers III, V, VI and IX were measured using a hand-held integrating sphere (ISP-REF, Ocean Optics B.V., Duiven, The Netherlands) connected to a fiber optic spectrometer (S2000, Ocean Optics). The S2000 spectrometer is equipped with a 2048 pixels Sony ILX511 CCD array detector. The wavelength resolution is determined by the instrument configuration. The installed grating has 600 lines/mm, is blazed at 400 nm and has a wavelength range of 650 nm. The optical resolution of this instrument configuration is 2.0 nm (FWHM). The overall system amplitude is influenced by factors such as detector response, fiber transmission characteristics, light source and the characteristics of the collection optics. However, the system has adequate sensitivity for reflectance spectroscopy. A typical integration time is 10 ms with a 5 W light source and a 2 m long collection fiber with 50 μm core diameter. See Fig. 3.2 for transmission characteristics. Due to drift, the spectrometer had to be re-calibrated frequently. The drift in the system may to some degree be controlled by allowing automatic software correction for electrical noise. The Ocean Optics spectrometer can be set to do consecutive scans and average the result before it is shown on the screen. The standard procedure with this equipment was to average ten scans and repeat all measurements three times. The warm up-time for this equipment was $5-10$ minutes.

The reflectance accessory from Labsphere consists of a Spectralon® integrating sphere with an internal halogen light source. The diameter of the integrating sphere is 7.6 cm and the entrance port diameter is 22 mm. Due to the light source, the signal to noise ratio is low for short wavelengths, and data below $380-400$ nm are therefore not included in the analysis of the measurements. This instrument is a typical lab equipment constructed for chemical analysis. The instrument is not easily portable, and the samples must be brought in contact with the aperture. Hence, it is difficult to control the amount of pressure applied against the aperture, and thus the blood flow in the measured area.

In reflectance spectroscopy the integrating spheres are used as light sources to achieve a Lam-
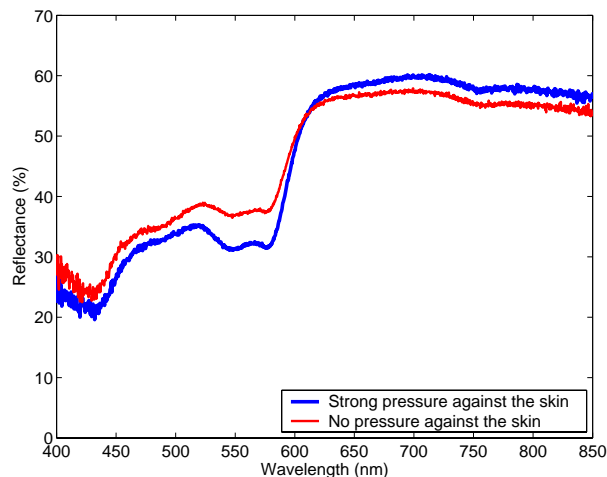
Figure 3.3: Typical reflectance spectra collected using different pressure against the skin. Measured using Ocean Optics ISP-REF. The spectra were collected at the same skin site.

bertian illumination of the sample. The illumination is dependent on the size of the sphere and the reflectivity of the coating inside the sphere. Direct illumination of the sample and the detector is avoided by baffling the light source. The HP-spectrometer has a large integrating sphere with a large aperture. This sphere has a strong integration of the light before it reaches the sample. However, the size of this sphere is also a drawback, since the measured signal is attenuated due to the longer path length of the photons before they reach the detector. The ratio of the port and sphere areas of this sphere meets the requirements of CIE for color measurements [58]. The Ocean Optics sphere is small, with a diameter of only 38 mm, the port diameter is either 20.0 mm or 10.3 mm. The sphere is coated with Spectralon. The sphere with the largest aperture size does not meet the CIE recommendations for color measurements due to the low ratio between reflective area and port area. The light is transmitted from the sphere to a fiber via a mirror and a SMA 905 fiber coupling. The fiber used was a standard multi mode UV-VIS fiber from Ocean Optics with a numerical aperture NA = 0.22. The transmission characteristics for the fiber is shown in Fig. 3.2.

Ideally, an integrating sphere should have a large reflective area and a large port area to assure good measurement quality. For wavelengths with a large penetration depth the light will penetrate deeper into the tissue and be scattered out of the collection angle of the integrating sphere, causing artifacts in the spectra, see Fig. 10 in paper IX. As a rule of thumb the aperture size should be at least 2 – 3 times the penetration depth to assure a good signal. The penetration depth in tissue is typical 3 – 5 mm in the red part of the spectrum.

The Ocean Optics sphere has the great advantage that it is hand-held and thus more flexible than the HP 8453 sphere in a practical measurement situation. The sphere being hand-held makes it easy to control the pressure applied during measurement. The pressure was always kept as low as possible to avoid blanching or erythema in the measured area. The effect of applying strong pressure onto the sphere during measurement is shown in Fig. 3.3. The temperature of the sphere surface is low on the Ocean Optics sphere; after the initial warm up time (5 minutes) the sphere holds approximately skin temperature. The Labsphere reflectance accessory is mounted in a position where the air circulation is low. The surface temperature therefore gets high enough to cause erythema after a measurement with 10 s integration time. The temperature on the surface must therefore be controlled by switching off the internal light source between the measurements. Typ-
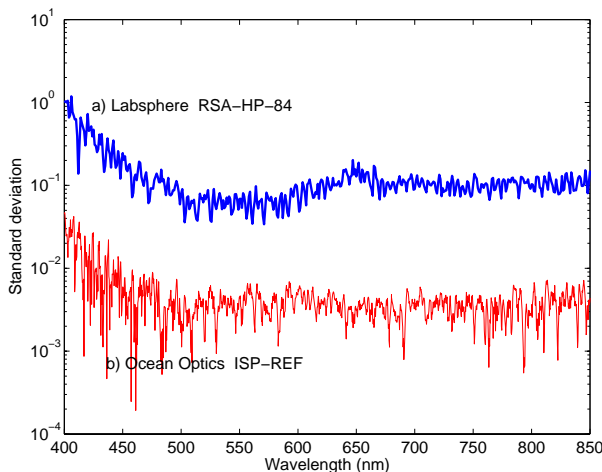
Figure 3.4: Typical standard deviation for reflectance measurements. a) HP8453 with Labsphere reflectance accessory; b) Ocean Optics SD2000 with ISP-REF integrating sphere.
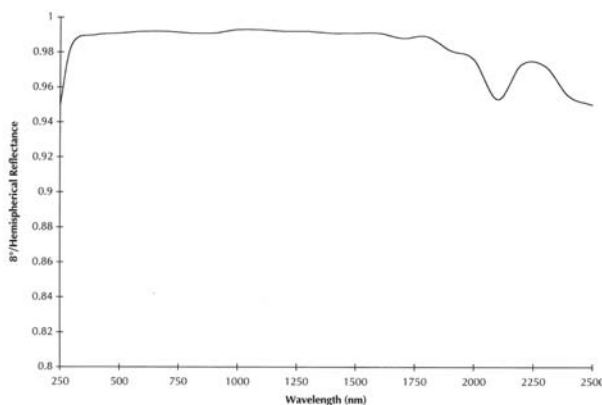
Figure 3.5: Reflectance of Spectralon material. Figure from data sheet.

ical standard deviation for reflectance measurements using the Ocean Optics and the Labsphere equipment is shown in Fig. 3.4. The smaller standard deviation for the Ocean Optics system is due to the averaging process which is incorporated in each measurement. If a measurement is recorded with the Ocean Optics system without averaging, the standard deviation would increase substantially.

The reflectance measurements were calibrated using polytetrafluoroethylene (PTFE) standards (SRS-90-010, Labsphere; WS-1 Diffuse Reflection Standard, Ocean Optics). Both standards are NIST traceable. Polytetrafluoroethylene (Spectralon®), see Fig. 3.5, is a diffuse white plastic that provides a highly Lambertian surface. This material reflects more than 98 % of light in the range 400 – 1500 nm and more than 95 % in the range 250 – 2000 nm [59]. The material has good long-term stability, is hydrophobic and chemically inert. The standard tiles are 10 mm thick and has a diameter of 32 mm. This reflection standard is assumed to be applicable for all the integrating sphere measurements included in this thesis.

The instruments described above are made to meet different specifications and different applications. The Hewlett Packard instrument is in my opinion a better, more reliable instrument than the Ocean Optics spectrometer, but is surpassed by the Ocean Optics system due to it's applicabil-

ity and hand-held nature. The Ocean Optics spectrometer fits in a back pack and can be brought easily from the lab to the bedside. However, it does require close attention of the user to assure that the calibration, settings and mounting are correct. For instance can a fiber connection that is not properly mounted destroy the whole measurement. To avoid such problems, I always start a measurement series by measuring the volar side of my forearm. This measurement works as a second calibration to check the software settings and calibration. The method presented in paper I is also applied to control for wavelength dependent drifting.

3.3   Individual variation in samples

Biological samples are fragile. *In vitro* tissue samples are vulnerable to changes in humidity, temperature and handling. However, these factors are controllable, and will be professionally handled by experienced laboratory personnel. A more subtle error is to assume that *in vitro* results are directly applicable for *in vivo* conditions. The work presented in *e. g.* paper II could not be assumed to have general validity, at least not before methemoglobin was identified *in vivo* (paper VI). In this case the methemoglobin formation is present in both cases, but the blood oxygenation probably differs notably. A blood sample exposed to air will maintain a high oxygenation. In tissue the blood is often found outside the vessels after laser exposure. In this case the oxygenation is limited by the available oxygen, and is therefore lower than in the *in vitro* case.

For *in vivo* measurements it is more difficult to handle the samples in a consistent manner. Alcohol, smoking and hormonal changes will influence on measured reflectance spectra. Alcohol might cause dilation of small vessels in the upper skin layers giving a blushing appearance, and thus lower reflectance levels. The day after alcohol consumption, the skin will be dehydrated, and the reflectance is reduced due to lower scattering. Smoking leads to contraction of the blood vessels and thereby leads to skin changes. Temperature and physical activity are also factors that may influence on reflectance measurements. Individual variations in pigmentation and scattering can also cause problems. The spectra shown in Fig. 3.6 is included to illustrate this effect. The data were collected on the volar side of the left forearm in healthy subjects. A measurement collected on the palm of the African volunteer is also included. The measurements were done in the same room with identical temperature conditions. In the spectrum measured on the fair skinned Caucasian female, betacarotene absorption can be seen at approximately 480 nm. This absorption might be mistaken for bilirubin absorption which also peaks in the same wavelength region. Day to day variations in the same individual has earlier been discussed by Norvang in her thesis [60]. Such changes are difficult to monitor if other causes of optical changes are present. It is therefore important to measure normal skin adjacent to the real area of interest to be able to quantify such changes.

The spectra presented in Fig. 3.7 are examples of optical changes caused by changes in medical condition. These spectra were measured on normal skin adjacent to a bruise in a heart surgery patient. These data were collected during the study presented in paper IX. This patient underwent coronary bypass surgery 2 days prior to the first measurement. In the first measurement the reflectance is low, with clearly visible oxyhemoglobin absorption. The patient was somewhat dehydrated and was given extra oxygen to breathe. In the second measurement the hydration is better, and the patient still receives extra oxygen. On the fourth day the extra oxygen has been removed, and deoxyhemoglobin absorption is clearly visible in the spectra. In the following days the condition of this patient improved significantly. These changes were also visible in the data

recorded in the bruised area, and could probably have caused a wrong conclusion regarding these data if the normal spectra were ignored.
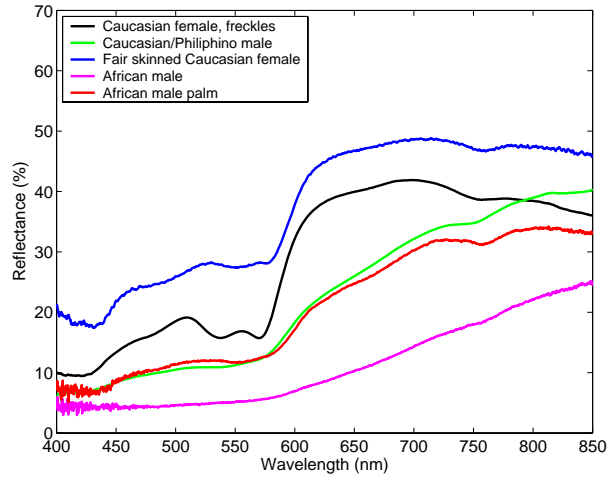
Figure 3.6: Reflectance spectra from different skin types, measured using the Ocean Optics SD 2000 with the ISP-REF integrating sphere with aperture diameter 10.3 mm.
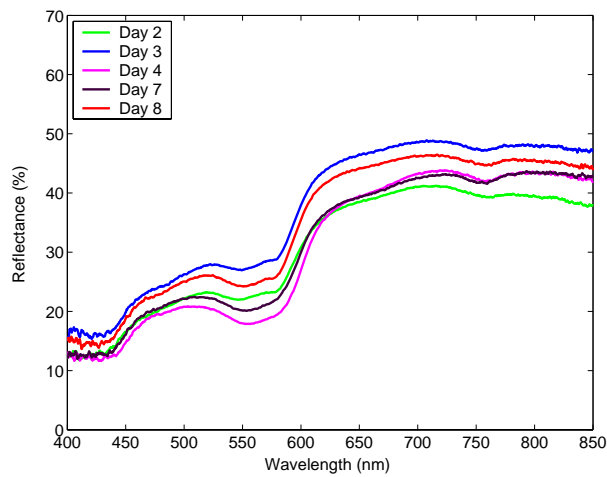
Figure 3.7: Variation in reflectance level as a function of time after coronary bypass surgery (day 0).

Chapter 4

Theoretical models

"As far as the laws of mathematics refer to reality, they are not certain; and as far as they are certain, they do not refer to reality."

Albert Einstein

MATHEMATICAL models are important tools to any scientist. To be able to take advantages of theoretical models, one must be aware of their limitations and be able to interpret the results they provide in the right context. In this chapter I have chosen to focus on two of the models used in this thesis. The optical photon transport model has been essential to my work. I have used both the two layer and three layer models extensively. The other model reviewed below is the new model for blood distribution in bruised tissues. This model is a first approach to describe the time development of a hemorrhage mathematically. Both models are based on diffusion theory and were mainly developed by professor Svaasand.

4.1   Photon transport in skin

Tissue is a complex and inhomogeneous structure. In skin, scattering exceeds absorption for wavelengths in the visible and near infrared parts of the electromagnetic spectrum. Ideally, photon transport in tissue should be described by solving Maxwell's equations with a proper set of boundary conditions. However, the structure and properties of skin make this difficult. Due to the complexity of the material and the boundary conditions, an exact solution would require tremendous amounts of computational power. Currently, the best approach is to describe the photon transport macroscopically. Methods like radiative transport theory and Monte Carlo methods have proven valuable in this context. In radiative transport theory Boltzmann's transport equation is derived by considering energy conservation and transport rather than electric and magnetic fields as in Maxwell's equations. However, an exact solution of the transport equation is also difficult to achieve without applying approximations, both to the mathematics and to the physical models involved.

If scattering dominates over absorption, optical diffusion theory can be applied [20]. Diffusion theory has a limited validity for thin layers, and it can be difficult to find appropriate boundary conditions especially for the boundary between air and tissue, since diffusion theory in this case

has no validity within air. For thicker structures, the reflected light has contributions from deeper tissue layers and a set of approximate boundary conditions can be found. The work by Haskell et al. [61] presented a set of such boundary conditions that have been proved to give good results in simulations of diffuse skin reflectance [1]. These boundary conditions have also been applied in the diffusion theory simulations included in this thesis.

4.1.1 Skin model

To apply a mathematical model on a physical structure, the physical structure must in most cases be simplified. A skin model that incorporates all inhomogeneities and structures of skin would be impossible to handle mathematically. The necessary complexity of the model is determined by the application. The diffusion models used in this thesis consist of two or three layers. The first model is really a one layer model, where a finite, flat layer representing the epidermis is put on top of a semi-infinite region. In the tree layer model the epidermal layer is followed by another finite layer on top of the semi infinite region. In the mathematical modeling of bruised skin the total thickness of the dermis is also given. The layers in the models are flat, and to incorporate the effect of the papillary structure, a small amount of blood has been added to the epidermal layer. All chromophores are simulated as homogeneously distributed within each layer. The dermal chromophores are incorporated into the model on basis of their respective volume fractions within the layer.

4.1.2 Diffusion theory

A diffusion model for skin was developed by Svaasand et al. [1] for port-wine stain diagnosis, and further refined by Spott and Svaasand [62]. The summary included here is based on references [1, 62].

Only approximate solutions can be found to Bolzmann's transport equation when the scattering is much stronger than the absorption *i. e.* $\mu_s \gg \mu_a$ [20]. One of these approximations is the diffusion approximation. The diffusion approximation assumes an almost isotropic light distribution within the tissue. In this case the radiance L can be expressed by a series expansion

$$L = \frac{\phi}{4\pi} + \frac{3}{4\pi}\mathbf{j} \cdot \mathbf{l} + \ldots \tag{4.1}$$

where $\mathbf{j}$ is the diffuse photon flux vector and ϕ is the fluence rate. The first term in the series expansion is the isotropic radiance, and the second term is the deviation from isotropy in the direction given by the unit directional vector $\mathbf{l}$. The irradiance on a surface normal to the flux can be expressed

$$E = \frac{\phi}{4} \pm \frac{j}{2} \tag{4.2}$$

The plus sign is valid for a surface facing against the flux, and the minus sign is valid for a surface facing along the flux. The diffuse photon flux vector $\mathbf{j}$ is given by Fick's law

$$\mathbf{j} = -\zeta \nabla \phi \tag{4.3}$$

The diffusion constant ζ is given by

$$\zeta = \frac{1}{3\mu_{tr}} = \frac{1}{3(\mu_s(1-g) + \mu_a)} \tag{4.4}$$

where μ_{tr}, μ_s g and μ_a are the transport coefficient, the scattering coefficient, the anisotropy factor and the absorption coefficient, respectively. Under steady state conditions the continuity equation can be expressed as

$$\nabla \cdot \mathbf{j} = -\mu_a \phi + q \tag{4.5}$$

where q is the source density for diffuse photons. Equations (4.3) and (4.5) can be combined to give the steady state diffusion equation

$$\nabla^2 \phi - \frac{\phi}{\delta^2} = -\frac{q}{\zeta} \tag{4.6}$$

where the optical penetration depth δ is given by

$$\delta = \sqrt{\frac{1}{3\mu_{tr}\mu_a}} \tag{4.7}$$

The boundary conditions between two scattering media can be expressed by the continuity of the irradiance in forward and backward direction

$$
\begin{aligned}
\frac{\phi_1}{4} + \frac{j_1}{2} &= \frac{\phi_2}{4} + \frac{j_2}{2} \\
\frac{\phi_1}{4} - \frac{j_1}{2} &= \frac{\phi_2}{4} - \frac{j_2}{2}
\end{aligned}
\tag{4.8}
$$

For the boundary between air and tissue a suitable boundary condition can be found by equating the reflected part of the irradiation at the tissue/air boundary to the irradiation propagating back into the skin [61]

$$R_{eff}\left(\frac{\phi}{4} + \frac{j}{2}\right) = \frac{\phi}{4} - \frac{j}{2} \tag{4.9}$$

where R_{eff} is the effective reflection coefficient. The value of R_{eff} is found by integrating the Fresnel reflection coefficient for un-polarized light with respect to all angles of incidence from within the tissue, see Sec. 4.1.4. The effective reflection coefficient becomes $R_{eff} = 0.431$ or $R_{eff} = 0.493$ for a refractive index of $n = 1.33$ and $n = 1.40$, respectively. This condition can also be expressed as

$$j = A\phi = \frac{(1 - R_{eff})}{2(1 + R_{eff})}\phi \tag{4.10}$$

The flux have to be less than the fluence rate for the optical diffusion theory to be valid. This condition is only partly fulfilled at the skin surface where $A = 0.2 - 0.17$ for $n = 1.33 - 1.44$ [61]. However, the ratio between the flux and the fluence rate is small enough to justify the use of optical diffusion theory [61].

4.1.3   Source functions and solutions

In a two layer skin model the upper (epidermal) layer has a finite thickness d_e, while the other layer is considered as semi-infinite. A small fraction of the incident light is reflected specularly at

the surface, and the rest of the light is transmitted into the tissue. The transmitted light is multiply scattered by the tissue constituents, and will eventually obtain an isotropic distribution. The source functions q_e and q_d for epidermis and dermis, is given by

$$
\begin{aligned}
q_e &= P_t\mu'_{s,e}e^{-\mu_{tr,e}x} &&: 0 < x \le d_e \\
q_d &= P_t\mu'_{s,d}e^{-\mu_{tr,e}d_e}e^{-\mu_{tr,d}(x-d_e)} &&: d_e < x \le \infty
\end{aligned}
\tag{4.11}
$$

where P_t is the transmitted fraction of the incident light, and $\mu'_{s,e} = \mu_{s,e}(1-g)$ and $\mu'_{s,d} = \mu_{s,d}(1-g)$ are the reduced scattering coefficients in epidermis and dermis, respectively. The solution of Eq. (4.6) is then given by

$$
\phi_e = \frac{P_t\delta_e^2\mu'_{s,e}}{\zeta(1-\mu_{tr,e}^2\delta_e^2)}e^{-\mu_{tr,e}x} + A_1e^{-\frac{x}{\delta_e}} + A_2e^{\frac{x}{\delta_e}}
\tag{4.12}
$$

$$
\phi_d = \frac{P_t\delta_d^2\mu'_{s,d}}{\zeta(1-\mu_{tr,d}^2\delta_d^2)}e^{-\mu_{tr,e}d_e}e^{-\mu_{tr,d}(x-d_e)} + A_3e^{-\frac{x}{\delta_d}}
\tag{4.13}
$$

The constants A_1, A_2 and A_3 are found by applying the boundary conditions given in Eq. (4.10) for the air/tissue boundary and the boundary condition given in Eq. (4.8) on the boundary between epidermis and dermis. The diffuse reflection coefficient for skin can thus be expressed

$$
\gamma = \frac{j|_{x\to 0}}{P_t}
\tag{4.14}
$$

The complete expression for γ is given by Svaasand et al. [1]. The model given above is the most basic model, the three layer model used in paper IX follows the same principles but includes additional terms for the third layer. The two layer model was as mentioned earlier found to work well for port-wine stain simulations. However, the applied source function was thought to deposit the energy at to shallow skin depths, especially for the high absorption case. Hence, Spott and Svaasand [62] made an effort to improve the model by implementing the δ-Eddington source function in the two layer model. This source function is more forward directed and deposits the energy at larger depths than the isotropic source function. This source function was intended to work better for highly absorbing tissue, and was applied for all two layer model simulations included in this thesis. For simulations with the three layer model, the isotropic source function was used. Recently the δ-Eddington has been implemented in the three layer model, and this source function will soon be tested on simulations of bruised skin. The δ-Eddington source function for epidermis and dermis is given below

$$
\begin{aligned}
q_e &= P_t\mu_{s,e}(1-g^2)e^{-(\mu_{s,e}(1-g^2)+\mu_{a,e})x} &&: 0 < x \le d_e \\
q_d &= P_t\mu_{s,d}(1-g^2)e^{-(\mu_{s,e}(1-g^2)+\mu_{a,e})d_e}e^{-(\mu_{s,d}(1-g^2)+\mu_{a,d})(x-d_e)} &&: d_e < x \le \infty
\end{aligned}
\tag{4.15}
$$

The solutions to Eq. (4.6) follows the same pattern as for the isotropic source function and are given as

$$
\phi_e = \frac{P_t\delta_e^2\mu_{s,e}(1-g^2)}{(1-\mu_{tr,e}'^2\delta_e^2)}\left(\frac{1}{\zeta} + 3\frac{g\mu'_{tr,e}}{1-g}\right)e^{-\mu'_{tr,e}x} + A_1e^{-\frac{x}{\delta_e}} + A_2e^{\frac{x}{\delta_e}}
\tag{4.16}
$$

$$
\phi_d = \frac{P_t\delta_d^2\mu_{s,d}(1-g^2)}{(1-\mu_{tr,d}'^2\delta_d^2)}\left(\frac{1}{\zeta} + 3\frac{g\mu'_{tr,d}}{1-g}\right)e^{-\mu'_{tr,d}d_e}e^{-\mu'_{tr,d}(x-d_e)} + A_3e^{-\frac{x}{\delta_d}}
\tag{4.17}
$$

where $\mu'_{\text{tr}} = \mu_s(1 - g^2) + \mu_a$ for the respective layers.

4.1.4 Fresnel reflection/specular reflection

As mentioned in Sec. 4.1.2 the effective reflection coefficient, R_{eff} can be found by integrating the expression for the Fresnel reflection coefficient with respect to all angles of incidence from the inside of the medium [61]. For non-polarized light

$$R_{\text{eff}} = \frac{R_\phi + R_j}{2 - R_\phi + R_j} \tag{4.18}$$

$$R_\phi = 2 \int_0^{\frac{\pi}{2}} \sin(\theta) \cos(\theta) R_F(\theta) \, d\theta \tag{4.19}$$

$$R_j = 3 \int_0^{\frac{\pi}{2}} \sin(\theta) \cos^2(\theta) R_F(\theta) \, d\theta \tag{4.20}$$

$$R_F(\theta) = \begin{cases} \frac{1}{2} \left(\frac{n \cos\theta' - n_{\text{out}} \cos\theta}{n \cos\theta' + n_{\text{out}} \cos\theta} \right)^2 + \frac{1}{2} \left(\frac{n \cos\theta - n_{\text{out}} \cos\theta'}{n \cos\theta + n_{\text{out}} \cos\theta'} \right)^2 & : 0 \leq \theta \leq \theta_c \\ 1 & : \theta_c \leq \theta \leq \frac{\pi}{2} \end{cases} \tag{4.21}$$

The angle of incidence θ from inside the tissue is given by $\cos\theta = \mathbf{s} \cdot \mathbf{n}$, where $\mathbf{s}$ is the direction of incidence on to the surface. The scattering angle θ' in the medium outside satisfies Snell's low, $n \sin\theta = n_{\text{out}} \sin\theta'$. The critical angle for total internal reflection, θ_c is given by $n \sin\theta_c = n_{\text{out}}$. For normal incidence Eq. (4.21) is simplified to

$$R_F(\theta = 0) = \left(\frac{n - n_{\text{out}}}{n + n_{\text{out}}} \right)^2 \tag{4.22}$$

The expression for the Fresnel reflection is used both to calculate the amount of specular reflected light at the skin surface, and to find the amount of light reflected against the surface from inside the tissue. For air $n_{\text{out}} = 1$ and with a refractive index in tissue $n = 1.4$, the border air/tissue has $R_{\theta=0} = 2.8\,\%$. This gives a critical angle of $45.6°$. The reflection coefficient decreases from 1 at an angle of incidence of $90°$ to $R_0 = 0.028$ for normal incidence [63]. The Fresnel reflection R_F behaves differently at the air and tissue sides of the boundary. At the tissue/air boundary total internal reflection will occur for incident angles larger than θ_c. This gives an imaginary k-vector and hence an exponentially damped evanescent wave propagating along the boundary.

4.2 Blood distribution in bruised tissue

4.2.1 Transport of hemoglobin in dermis

A crushing type of tissue injury will result in bleeding from damaged vessels. In most bruises damages are confined to smaller vessels such as arterioles and venules. A localized damage may rapidly result in a pool of blood in subcutaneous tissues, which subsequently is transported deeper into tissue. Blood will flow easily along the interspaces between muscle bundles and membranes as well as along and across muscle fibers. The total extravascular transport of hemoglobin in tissue can thus be expressed by convection and diffusion,

$$j_i = -D_{ik} \frac{\partial N}{\partial x_k} - \xi K_{ik} \frac{\partial p}{\partial x_k} \tag{4.23}$$

where j_i is the component of the hemoglobin flux vector, D_{ik} is the hemoglobin diffusivity tensor, K_{ik} is the Darcy constant for whole blood and ξ is the volume fraction of hemoglobin in whole blood, *i. e.* $\xi = 0.14 - 0.15$ corresponding to a hemoglobin concentration of $140 - 150$ g/l. After the initial phase, hemoglobin will be transported into dermis by diffusion from the subcutaneous layer of whole and hemolyzed blood. The transport mechanism is in the present model supposed to be primarily of diffusive character. When the Darcy term in Eq. (4.23) is neglected the transport flux vector in an isotropic medium becomes,

$$\mathbf{j}_H = -D_H \nabla N_H \tag{4.24}$$

where D_H is the hemoglobin diffusivity and N_H is the density of molecular hemoglobin. The continuity of hemoglobin in a medium with loss can be expressed,

$$\nabla \cdot \mathbf{j}_H = -\frac{\partial N_H}{\partial t} - \frac{N_H}{\tau_H} \tag{4.25}$$

where t is time and τ_H is the hemoglobin relaxation time. This lifetime is determined by several mechanisms such as drainage by the lymphatic system, conversion to bilirubin/bilirubin or consumption by macrophages. The relaxation time can be expressed,

$$\frac{1}{\tau_H} = \frac{1}{\tau_L} + \frac{1}{\tau_B} + \frac{1}{\tau_M} + \dots \tag{4.26}$$

where τ_L, τ_B, and τ_M are the relaxation times due to lymphatic drainage, conversion to biliverdin/bilirubin and to macrophage activity, respectively.

There is very limited information on *in vivo* hemoglobin diffusivity in the literature. However, the diffusivity of myoglobin in skeletal muscle cell is reported to be $1.2 \cdot 10^{-11}$ m^2/s [64]. The molecular weight of hemoglobin (66 000 Dalton) is approximately four times as large as that of myoglobin (17 000 Dalton). Therefore the diffusivity of hemoglobin in skin is expected to be less than this value, and fitting the model with patient data indicate a diffusivity in the range of $D_H = 3 \cdot 10^{-12}$ m^2/s.

The relaxation time, also as determined from patients, is in the range of $\tau_H = 1.7 - 2.6 \cdot 10^5$ s ($2 - 3$ days). However, the relaxation time is observed to be significantly less in a region of $5 - 10$ mm around damaged vessels. Here, a whitish region is formed about $0.5 - 1$ day after injury, and this region expands with time. This phenomenon, which is assumed caused by macrophages from the damaged vessel, reduces the hemoglobin relaxation time to $\tau_H = 0.2 - 0.4 \cdot 10^5$ s ($0.25 - 0.5$ days).

4.2.2   Transport and generation of bilirubin in dermis

Diffusion of bilirubin in dermis can be expressed by a transport flux vector $\mathbf{j}_B$,

$$\mathbf{j}_B = -D_B \nabla N_B \tag{4.27}$$

where D_B is the bilirubin diffusivity and N_B is the density of molecular bilirubin. The transition from biliverdin to bilirubin is fast compared to other timescales of the system. Therefore, the generation of bilirubin can be characterized by the time τ_B, which characterizes the hemoglobin to bilirubin/biliverdin transition.

The continuity of bilirubin can be expressed,

$$\nabla \cdot \mathbf{j}_B = -\frac{\partial N_B}{\partial t} - \frac{N_B}{\tau_{BR}} + \frac{N_H}{\tau_B} \tag{4.28}$$

where τ_{BR} is the bilirubin relaxation time. If diffusion of bilirubin can be neglected Eq. (4.28) is simplified to,

$$\frac{\partial N_B}{\partial t} = -\frac{N_B}{\tau_{BR}} + \frac{N_H}{\tau_B} \tag{4.29}$$

4.2.3   Planar skin model

The diffusion of hemoglobin into dermis can be modeled as flow in a planar model. The diffusivity in epidermis is negligible, and the boundary condition at the basal layer can therefore be taken as zero flow. The sub-dermal hemoglobin source can, since the diffusion process is much slower than the process for distribution of blood in subcutaneous tissue, be taken to be instantaneously established at time $t = 0$. The spatial and temporal distribution of hemoglobin in dermis can be expressed by Eqs. (4.24) and (4.25) as

$$N_H(x,t) = N_{H0} \left\{ \sum_{n=0}^{\infty} \left[(-1)^n \mathrm{erfc}\left(\frac{(2n+1)d - x}{2\sqrt{D_H t}} \right) + (-1)^n \mathrm{erfc}\left(\frac{(2n+1)d + x}{2\sqrt{D_H t}} \right) \right] \right\} e^{-\frac{t}{\tau_H}} \tag{4.30}$$

where N_{H0} is the subcutaneous density of hemoglobin, x is the distance from the basal layer and d is the dermal thickness. The relaxation time of dermal hemoglobin and hemoglobin in the subcutaneous region are both assumed to be τ_H. The series in Eq. (4.30) converges rapidly, and for time scales where $t < 4d^2/D_H$ the two first terms give satisfactory accuracy,

$$N_H(x,t) = N_{H0} \left\{ \mathrm{erfc}\left(\frac{d - x}{2\sqrt{D_H t}} \right) + \mathrm{erfc}\left(\frac{d + x}{2\sqrt{D_H t}} \right) \right\} e^{-\frac{t}{\tau_H}} \tag{4.31}$$

The first of these terms represent diffusion into a semi-infinite medium and the second term represents a mirror source ensuring zero flux at the basal layer. The corresponding approximation for the average dermal hemoglobin distribution follows from integration of Eq. (4.31)

$$\overline{N_H}(t) = \frac{2N_{H0}}{d\sqrt{\pi}} \left\{ \sqrt{D_H t}\left(1 - e^{-\frac{d^2}{D_H t}} \right) - d\sqrt{\pi}\,\mathrm{erfc}\left(\frac{d}{\sqrt{D_H t}} \right) \right\} e^{-\frac{t}{\tau_H}} \tag{4.32}$$

The corresponding solution for bilirubin distribution in presence of diffusion in dermis can be established by forming a Green's function from the hemoglobin distribution, together with a mirror-distribution that establishes the criterion of no bilirubin transport into the epidermis. If all diffusion of bilirubin can be neglected, the solution of Eqs. (4.27) and (4.29) can be expressed as

$$N_B(x,t) = e^{-\frac{t}{\tau_{BR}}} \int_{\tau=0}^{t} \frac{N_H(x,\tau)e^{\frac{\tau}{\tau_{BR}}}}{\tau_B} d\tau \tag{4.33}$$

where $N_H(x,\tau) = N_H(x,t \to \tau)$ from Eqs. (4.30) or (4.31). When diffusion within the dermis is present and diffusion across the dermal/subcutaneous tissue border is neglected, the average bilirubin concentration for small values of time can be expressed as

$$\overline{N_B}(t) = \frac{N_{H0}\tau_{BR}\tau_H}{\tau_B(\tau_H - \tau_{BR})d} \left\{ 2\sqrt{\frac{D_H t}{\pi}} e^{-\frac{t}{\tau_H}} - \mathrm{erf}\left(\frac{(\tau_H - \tau_{BR})t}{\tau_{BR}\tau_H} \right)\sqrt{\frac{D_H\tau_{BR}\tau_H}{\tau_H - \tau_{BR}}} e^{-\frac{t}{\tau_{BR}}} \right\} \tag{4.34}$$

Chapter 5

Summary and discussion of included work

"The art of drawing conclusions from experiments and observations consists in evaluating probabilities and in estimating whether they are sufficiently great or numerous enough to constitute proofs. This kind of calculation is more complicated and more difficult than it is commonly thought to be."

Antoine Lavoisier

T HIS chapter contains a brief summary and discussion of the papers included in this thesis. It is not intended to give an in-depth analysis of each paper, but provides an overview of the main contributions in each paper. The papers have been grouped according their main area of focus, and for each area a short background and introduction is included to show the relation between the different papers. It is important to emphasize that the included discussion is subjective, and strongly flavored by my personal opinions.

5.1   Port wine stain diagnosis and treatment

An important topic of this thesis is port-wine stain diagnosis, treatment, and treatment monitoring. This part of the work is partly a follow up of Lill Tove Norvangs thesis [60]. It is also influenced by the close relation between our group in Trondheim and Beckman Laser Institute and Medical Clinic at UC Irvine.

Port-wine stains are congential birthmarks that are found in $0.3 - 0.6\,\%$ of all newborns. Such vascular lesions are often considered as a psychological burden [65] and are therefore subject to therapy. Currently, laser therapy is the preferred technique, although only about $25\,\%$ of the treated patients experience complete fading of their lesions [3, 66, 67]. Due to this lack of response in many patients, a large effort has been put into research on diagnostics, treatment monitoring and dosimetric aspects in port-wine stain treatment. Techniques for diagnostics, treatment monitoring and methods for thermal control of the skin during laser therapy are presented in this thesis. A special focus is put on the thermal dependence of the hemoglobin optical properties in connection with laser exposure.
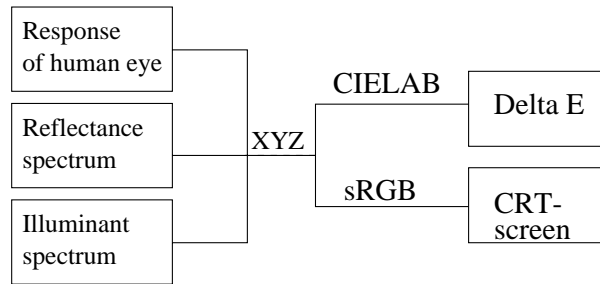
Figure 5.1: Calculation path from reflectance spectrum to color coordinates.

5.1.1   Paper I: Treatment monitoring

L.L. Randeberg, L.O. Svaasand, Simulated color: a diagnostic tool for skin lesions like port-wine stain, Proceedings of SPIE, 4244:1 – 12, 2001

This paper presents a method for visualization of skin color on a CRT screen. The aim of the work was to establish a reproducible, accurate method for objective evaluation of skin color and for electronic exchange of color information. It was also an aim to identify the relation between changes in the skin reflectance and perceivable color changes.

The motivation for this work was the fact that port-wine stain treatment often requires multiple laser sessions to obtain satisfactory results. Prolonged treatments without adequate response will cause the patients unnecessary pain, and will be of economic significance since laser treatments are expensive.

A device independent method for skin color visualization was developed based on translation of color information from measured reflectance spectra into standard Red Green Blue (sRGB) color coordinates [68] which are plotted on a CRT screen. The calculation path from reflectance spectrum to CRT screen is given in Fig. 5.1. The colors were presented as adjacent patches surrounded by a medium grey border. The border was included to serve as a calibration source for the visual system. The sRGB system was originally designed by Microsoft and HP [69], and has received wide adaption in the consumer imaging industry. This system is based on the typical colors of a CRT-screen. The strength of sRGB is its simplicity; it is inexpensive to implement, computationally efficient and transparent to the end users. The sRGB color space is a perceptual space, which means that it is optimized for linearity with the human visual system. This is one of the key features for this application of sRGB, where we are aiming at a system for objective skin color evaluation for users that are trained in direct visual inspection.

Change in skin color due to a change in average blood content or scattering properties in dermis was investigated, based on analytic simulations using a two layer photon transport model based on the diffusion approximation [1]. Color difference ΔE and CIELAB color coordinates (International Commission on Illumination) was used to evaluate the effect of varying the scattering and absorption in skin. It was found that a 11 % change in average blood content and a 15 % change in scattering properties gave a visible color change. The visibility limit for ΔE was found to be slightly below $\Delta E = 1$. The visibility limit was found based on experimental testing and known properties of the human visual system. The knowledge about the visibility limit can be used to determine when to terminate laser treatment of port-wine stain due to low treatment response, *i. e.* low ΔE between treatments. The visualization method presented seemed promising for medical applications as port-wine stain diagnostics, and gave good possibilities for electronic transfer of data between clinics because it is device independent.

This was the first paper written for this thesis, and the imaging technology and computer industry has experienced a fast development throughout the last five years. Due to problems with long distance cooperation and lack of possibility of day-to-day contact, the planned follow up study at the National Hospital of Norway (Rikshospitalet) was never carried out. This method may seem obsolete compared to modern digital photography and visualization techniques, although it can be adjusted to fit LCD screens. Personally, I still use this method to visualize colors as an immediate check of the calibration of the reflectance measurements and to identify changes in colors after laser treatment. Seen in retrospective the most important contribution in this paper was to identify the visibility limit, and the corresponding changes in scattering and absorption necessary for creating visible color changes.

5.1.2 Paper II: Thermal properties of human hemoglobin

L.L. Randeberg, A.J. Daae Hagen, L.O. Svaasand, Optical properties of human blood as a function of temperature, Proceedings of SPIE, 4609:20 – 28, 2002

This paper presents data on optical changes in hemoglobin during slow heating. The aim of this paper was to investigate the effect of slow heating on hemoglobin solutions. Emphasis was put on quantifying heat induced changes in absorption and scattering properties of human blood. Especially the correlation between thermal denaturation of hemoglobin and formation of methemoglobin was focused on.

Knowledge of optical and thermal properties of human tissue is essential for optimization of laser therapy and optical diagnostics. The temperature dependence of hemoglobin is important since it is the target chromophore for laser treatment of *e. g.* port-wine stains.

In the experimental part of this paper erythrocyte concentrate was heated for two minutes in a water bath, hemolyzed with distilled water and centrifuged before absorption spectra were collected. Measurements were performed in the range of $50 - 80\,°C$. Penetration depth measurements of the heated erythrocyte concentrate were done at 488 nm, 585 nm, 590 nm and 630 nm. For these measurements the erythrocytes were mixed with a highly scattering material (whole milk). The hemoglobin absorbance demonstrated a characteristic change during heating. This change was found to be partly due to oxidative reactions with formation of methemoglobin, and partly due to protein denaturation. The change in the absorption coefficient due to methemoglobin has a maximum at approximately $72\,°C$, where a $200\,\%$ increase was measured at 630 nm wavelength.

It was shown that heat induced changes of the optical properties of hemoglobin occur at temperatures exceeding $65\,°C$. This change in absorption properties is due to formation of methemoglobin caused by thermal stress and hemoglobin/methemoglobin denaturation. At temperatures above $75\,°C$ this reaction was found to occur within seconds. The formation of methemoglobin led to an enhanced optical absorption at several wavelengths *e. g.* 508 nm and 630 nm. Formation of methemoglobin was found to occur simultaneously with denaturation of hemoglobin and methemoglobin. Formation of methemoglobin dominates for temperatures below $72\,°C$, above this temperature the denaturation rate was found to increase and denaturation became the dominating process.

The work presented in this paper was induced by a question from professor Svaasand. He asked if I knew what happened to the optical properties of hemoglobin during heating. I couldn't answer his question and headed off to the lab with a blood sample to find out. The first evidence of optical changes occurred at 635 nm, where a substantial absorption maximum developed. A search in the literature identified this substance as methemoglobin, and the rest of the story is writ-

ten in the paper. This work was almost finished when Barton et al. [6] published their work, and was presented at BIOS 2002 in San Jose in the same session where Jennifer Barton presented their study on laser induced methemoglobin. The results of this study were of good quality considering the limited laboratory equipment that were available. The identification of methemoglobin following laser irradiation/heat exposure was a contribution to the understanding of the biological and thermal processes going on in skin during laser exposure. The article has been recognized, and was cited by Mordon et al. [70] and Ross and Domankevitz [71] in their articles on laser treatment of leg veins.

5.1.3   Paper VI: *In vivo* detection of methemoglobin

L.L. Randeberg, J.H. Bonesrønning, M. Dalaker, J.S. Nelson, L.O. Svaasand, Methemoglobin formation during laser induced photothermolysis of vascular skin lesions, Lasers Surg Med, 34(5): 414 – 419, 2004

This study presents a proof of concept of a method for monitoring the *in vivo* presence of methemoglobin immediately after laser exposure. The study is a follow up of paper II, where *in vitro* methemoglobin formation was investigated.

Emphasis was put on quantifying changes in hemoglobin absorption properties *in vivo* in the $450 - 800$ nm wavelength region. Measurements of diffuse reflectance on port-wine stain and telangiectasia were performed prior to, and immediately after laser treatment with a pulsed dye laser (PDL) at 585 nm wavelength. Changes in optical properties of hemoglobin *in vivo* were evaluated based on the reflectance data.

In vivo measurements showed immediate increase in the optical absorption in human skin following laser treatment. This effect, caused by thermal stress, was a result of an increased dermal blood volume fraction and methemoglobin formation. The effect was found to be dependent on light dose, and reflectance spectra revealed methemoglobin formation in patients treated with fluences above 5 J/cm^2 at 585 nm wavelength. The spot size and pulse length were 7 mm and 0.45 ms, respectively. The methemoglobin formation was identified by using the first derivative of the reflectance spectrum compared to simulated spectra with a known distribution of hemoglobin species.

It was proved by the present study that methemoglobin can be measured *in vivo* by reflectance spectroscopy. Measurements of average methemoglobin concentration immediately after laser exposure was suggested to be a valuable diagnostic tool to verify that the blood temperature has been sufficiently high to induce thermal damage to the vessel wall. A temperature of at least 70 °C is needed to achieve permanent destruction of the vessel wall in the target vessels. Immediate information about vessel damage can be acquired utilizing the temperature dependence of methemoglobin formation. This is due to the fact that methemoglobin is formed in measurable amounts at temperatures high enough to destroy the vessel walls, as was found in paper II.

In conclusion, the present study was a proof of concept, and future work will include studies on the relation between average methemoglobin concentration measured immediately after laser therapy and the blanching response of port-wine stain and other vascular lesions. A follow up study at Trondheim University Hospital has been briefly discussed and will be initiated depending on financial support of the project.

This article was the first article to prove *in vivo* formation of methemoglobin following laser exposure. The paper has been acknowledged and cited by other authors [72, 73]. However, the value of this study has also been questioned by Black et al. [74], with the argument that the

oxygenation values used in the simulations were unrealistic in an *in vivo* situation. This is despite the fact that the oxygenation in skin can be estimated from the reflectance spectrum, and therefore is a controllable parameter.

5.1.4 Paper IV: Cooling efficiency of cryogen spray cooling

L.O. Svaasand, L.L. Randeberg, G. Agiular, B. Majaron, S. Kimel, E.J. Lavernia, J.S. Nelson, Cooling efficiency of cryogen spray during laser therapy of skin, Lasers Surg Med, 32(2):137 – 142, 2003

This paper presents a method to measure the heat transfer coefficient during cryogen spray cooling (CSC) of skin prior to laser treatment. The aim of this study was to construct and build a detector to perform reliable measurements of the heat transfer coefficient.

Cryogen spray cooling is used extensively for epidermal protection during laser-induced photothermolysis of port-wine stain and other vascular skin lesions. The efficacy of CSC depends critically on the heat transfer coefficient (H) at the skin surface.

A simple experimental model was designed and constructed, consisting of a pure silver measuring disk (diameter 10 mm, thickness *e. g.* 1 mm), embedded in a thermal insulator. The disk temperature was measured by a Chromel-Alumel thermocouple soft-soldered to the lower surface. The upper disk surface was exposed to cryogen with a spray diameter 50 % larger than that of the disk. Disks had a thickness of 0.7, 1.0, or 2.0 mm. The small ratio between thickness and diameter ensures that the temperature distribution and heat flow in the disk could be treated as one-dimensional. The disk was covered with a 10 μm thick stratum corneum layer, detached from *in vivo* human skin. The heat transfer coefficient of the stratum corneum/cryogen interface was measured during CSC with short spurts of atomized tetrafluoroethane. The heat transfer coefficient was found to be dependent on the specific design of the cryogen valve and nozzle. With nozzles used in typical clinical settings, H was 11 500 W/m^2 K, when averaged over a 100 ms spurt, and 8 000 W/m^2 K when averaged over a 200 ms spurt. The presented model enabled accurate prediction of H and thus improved control over temperature depth profile and cooling efficiency during laser therapy. Thus, it may contribute to improvement of therapeutic outcome.

When this idea was first introduced by professor Svaasand it was very controversial. It was questioned whether a metal detector could be used to measure the heat transfer coefficient during skin cooling. The main reason for this objection was the fact that the thermal conductivity is much larger in silver than in skin, and thus would impact on the results. The high conductivity disk material was chosen to achieve a homogeneous temperature distribution within the disk almost instantaneously. This uniform temperature distribution allowed simple one-dimensional mathematical treatment of the disk temperature as a function of time, and hence the calculation of the heat transfer coefficient. A finite disk thickness gives the possibility to match the thermal flux of the disk to that of a semi-infinite skin layer for the duration of the cryogen spurt. The heat transfer coefficient in the disk is determined by the disk thickness and the specific heat of the disk, whereas in skin the amount of heat transfered to the tissue depends on the thermal diffusivity. When all these conditions are controlled, the dynamic temperature profile of the disk could be used to extract the heat transfer coefficient for skin from measurements using the silver detector.

My contribution to this work was limited mainly to the experimental part of the study. The experiments were carried out at a Beckman Laser Institute in cooperation with professor Svaasand and Boris Majaron. The analysis of the data was done by me in Trondheim based on a Excel worksheet made by Boris Majaron.

5.1.5 Paper VII: Manipulating optical properties prior to treatment

L.O. Svaasand, G. Aguilar, J.A. Viator, L.L. Randeberg, S. Kimel, J.S. Nelson, Increase of dermal blood volume fraction reduces the threshold for laser-induced purpura: Implications for port wine stain laser treatment, Lasers Surg Med, 34(2):182–188, 2004

This paper presents a study on the effect of occluding the blood supply to the extremities to increase the dermal blood volume fraction prior to laser treatment. The aim of this study was to investigate a potential technique for more efficient photocoagulation of small diameter blood vessels in port-wine stains (PWS) that respond poorly to selective photothermolysis.

The average success rate in achieving total blanching of PWS lesions treated with laser-induced selective photothermolysis is below 25 %, even after multiple treatments. This is because smaller diameter ($5-20\,\mu$m) blood vessels are difficult to destroy with selective photothermolysis since the volumetric heat generated by absorption of laser light is insufficient to adequately heat the entire vessel wall.

In the experimental part of this work the blood volume fraction (BVF) in the upper dermis of the forearm of human volunteers was increased by placing an inflated blood pressure cuff on the upper arm. Applied pressures were in the range of $80-100$ mmHg for up to 5 minutes. The increased BVF was determined by matching measured reflectance spectra with spectra computed using a diffusion model. The impact of increased BVF on purpura formation induced by a 0.45 ms pulsed dye laser (PDL) at 585 nm wavelength was investigated in normal and PWS skin.

In the presence of a 100 mmHg pressure cuff, the BVF determined from the diffusion model increased by a factor of 3 in the forearm and by 6 in the hand. Increasing BVF by a factor of 3 corresponds to an increase in blood vessel diameters by a factor of $\sqrt{3} \approx 1.7$. BVF increased for $1-3$ minutes after application of the pressure cuff, remained constant for $3-5$ minutes, and returned to baseline values 3 minutes after removal of the pressure cuff. Approximately 40 % less radiant exposure was needed to induce the same amount of purpura after PDL irradiation when the blood pressure cuff was used. Applying an 80 mmHg pressure cuff reduced the required radiant exposure for purpura formation by 30 %. Heating of blood vessels was calculated as a function of vessel diameter and of radiant exposure (at 585 nm and with 0.5 and 1.5 ms pulse duration). Enlarging the vessel lumen, *e. g.* by obstructing venous return, can significantly reduce the "small-vessel-limitation" in PDL treatment of PWS. Dilation of PWS blood vessels enables a more efficient destruction of smaller vessels without increasing the probability of epidermal damage.

This technique has a limited applicability since the vessels have to be occluded using a pressure cuff. This limits the method to the extremities, and a suction technique was therefore tested to achieve the same effect. In this method a vacuum pump was used to create a dilatation of the vessels in the treatment area.

Most of the work in this paper was carried out at Beckman Laser Institute during professor Svaasand's sabbatical in 2002/2003. I contributed to this work by doing initial measurements of the increase in dermal BVF following vacuum treatment of a small skin area. The results from these preliminary measurements were considered as so promising that a full study was initiated.

5.2 Optical properties of tissue

The first preliminary draft of my PhD project was titled "Optical and thermal properties of human tissue", and the idea was to develop a data bank of optical properties of human tissue. With time,

the focus of my project moved away from this title. However, knowledge of optical data of the tissue in question is of great importance to all fields of optical diagnostics.

The two papers presented in this part of the thesis considers optical diagnostics of human liver tissue (paper III), and optical diagnostics of neonatal jaundice (paper VIII).

5.2.1 Paper III: Optical properties of human liver tissue

L.L. Randeberg, O.A. Haugen, L.O. Svaasand, Optical diagnostics of liver pathology, Proceedings of SPIE, 5141:187 – 195, 2003

This paper presents preliminary results on the applicability of reflectance spectroscopy and color coordinates in quantitative optical diagnosis of liver pathologies. The aim of the study was to determine whether reflectance spectroscopy could be an alternative to traditional histology.

Pathological changes in the liver can result from *e. g.* prolonged alcohol abuse, diabetes or obesity [75, 76]. Diabetes and obesity are major health problems in most western countries. Many pathologic liver changes are reversible if the cause of the changes is removed, and accurate diagnostic methods are therefore important. The characteristic accumulation of fat inside liver cells seen in fatty liver affects the optical properties, and are therefore evident in diffuse reflectance spectra. Thus, reflectance spectroscopy can be used for quantitative evaluation of fat content in hepatic tissue. Similarly, due to optical changes caused by the presence of connective tissue, such tissue changes can also be quantified.

The experimental work was carried out at Trondheim University Hospital. Post mortem reflectance spectra were collected from liver tissue originating from 13 individuals. A point counting method was applied to determine relative areas of connective tissue, liver cells with or without fat vacuoles, and vascular spaces in the liver. CIELAB color coordinates were used to quantify the reflectance changes in the measured samples.

This study shows the potential of reflectance spectroscopy to assess morphological changes in liver tissue. Optical diagnostic techniques can provide a low-cost method for quantifying pathological changes in liver tissue. These techniques can be utilized during minimal invasive surgery for quick on-site diagnosis by collecting reflectance spectra with a fiber probe during laparoscopy. However, the invasive nature of reflectance measurements on inner organs is a major drawback for the applicability of this technique. Other techniques like ultrasound, CT and MRI are also of limited use for diagnosis in these conditions. Ultrasound may show a bright signal, but may also appear normal, CT shows a reduced attenuation, and MRI show fatty changes in some cases. So far sampling of liver biopsies is the best method to diagnose fatty changes in the liver [75], and since this is an invasive technique, reflectance spectrometry still provides an alternative.

The experimental part of this study was challenging. The first idea was to do a broad study on a variety of human tissue samples, and present an overview of the optical properties within the samples. However, the experiments were cumbersome and the number of samples were limited. The reflectance data were collected using an integrating sphere, and the combination of a technique which requires contact between sample and probe, and autopsy material, was not ideal. Test measurements with a more robust fiber probe were initiated, but were not successful, since the fiber probe results depended strongly on the probe position. The limited collection angle of the fiber probe also caused loss of red light from the reflectance spectrum. These problems could possibly have been overcome by building a probe holder and making a permanent set-up. Unfortunately, it was not possible to do so in this setting. The measurements were carried out in the autopsy room at the hospital, and the equipment had to be removed every afternoon. The most

promising results from this study were the liver data, presented in this paper. The reflectance difference between normal samples and tissue samples with morphological changes were prominent, and agreed well with the histology data. The results in this study are preliminary, and the study should be expanded to achieve statistically significant values.

5.2.2   Paper VIII: *In vivo* spectroscopy of hyperbilirubiemia in newborns

L.L. Randeberg, E.B. Roll, L.T. Norvang Nilsen, T. Christensen, L.O. Svaasand, In vivo spectroscopy of newborn skin reveals more than a bilirubin index, Acta Paediatrica, 94(1):65 – 71, 2005

In this paper reflectance spectroscopy is used to quantify the degree of hyperbilirubinemia and to monitor physiological changes during light therapy. Emphasis is put on evaluating pigmentation and blood oxygenation levels in the skin at various body sites. The aims of this study were to investigate the algorithms for calculating the transcutaneous bilirubin index (TcB), to monitor bilirubin concentration during phototherapy, and to evaluate light induced skin changes such as pigmentation and erythema during phototherapy.

This paper resulted from a cooperation with Ellen Bruzell, Terje Christensen and Lill Tove Norvang Nilsen at the Norwegian Radiation Protection Authority. Paper VIII was also included in the Dr. Scient thesis of Ellen Bruzell. The initial work in this project was carried out by Thorsten Spott in his thesis [40]. After his dissertation the project was taken over by me.

Neonatal jaundice is seen in almost every second baby. About $5 - 10\%$ of the cases require therapy to avoid brain damage due to accumulation of toxic bilirubin. Bilirubin can be measured transcutaneously due to a characteristic absorption peak at 460 nm. Non-invasive techniques for monitoring of neonatal jaundice have improved over the last 40 years. The first icterometer based on visual inspection was introduced in the 1960s. This simple device was followed by two-wavelength reflection bilirubinometers. The newest device, BiliCheck, is based on reflectance spectroscopy. This device collects reflected light from a range of wavelengths, enabling mathematical corrections of physiological variations. Reflectance spectroscopy enables measurement of bilirubin concentration in both blood and tissue. Due to the variation in light penetration at the wavelengths emitted from the instrument, light is back-scattered from various layers in the skin. Light induced skin changes during phototherapy can be monitored using reflectance spectroscopy, *e. g.* by determining the erythema and melanin indices.

Reflectance measurements were performed on 51 jaundiced newborns of which 10 were given phototherapy. The measurements were collected with a diode array spectrometer with an integrating sphere accessory, and a TcB was calculated from the measured spectra using algorithms based on diffusion theory. Heel stick blood samples were analyzed for total serum bilirubin (Sbr). Measurements from the forehead gave the best correlation between TcB and Sbr ($r = 0.81$, $p < 0.05$). However, no significant correlation between TcB and Sbr was observed during phototherapy. A correlation ($r = 0.45$, $p < 0.05$) was found between phototherapy and melanin index obtained from the patients' back.

Reflectance spectroscopy was found useful in assessing bilirubin concentrations before phototherapy, and did also reveal changes in skin parameters, *e. g.* pigmentation occurring as a result of phototherapy.

This article was written based on an analysis of data recorded by Peter Schmedling during his diploma thesis in 1996. I got these data from Thorsten Spott in 1999/2000, but kept them in my drawer for years before they were analyzed. When the data finally were analyzed they revealed

interesting findings on the physical properties of infant skin during phototherapy. This paper also utilizes a method to calculate the blood oxygenation from the reflectance spectra. When the oxygenation is calculated at wavelengths with different penetration depths, it represents the oxygenation in different skin layers. Hence, the method gives the integrated oxygenation from the surface down to a certain depth depending on the penetration depth. The oxygenation was found to vary slightly with body site for both shallow and deeper skin depths. This method has proved to be valuable to find input parameters for analytic simulations, as shown in paper IX.

5.3   Forensic optics

This part of the thesis is to some degree a follow up of papers III, VI and VIII. The work initiated as a result of the cooperation with the department of pathology at Trondheim University Hospital. Professor Olav A. Haugen was our collaborator at the hospital and provided the tissue samples for paper III. The idea of doing optical analysis of bruises was proposed by him as a response to my review of my earlier work on neonatal jaundice, since bilirubin also is an important contributor to the appearance of skin hematomas or bruises. This work is a interdisciplinary challenge, depending on medical as well as technical knowledge. The analysis of bruises utilizes the methods developed during the work with papers VI and VIII.

Forensic experts are often confronted with questions regarding the age of injuries in abuse cases. The preferred techniques to estimate the age of skin hematomas are either direct visual inspection or inspection of photos [77, 78, 79]. These methods rely on the experience of the examiner and might be disturbed by factors like ambient lighting or photo quality. Several authors have discussed the problem of determining the age of bruises [77, 78, 80, 81], and Stephenson and Bialas [78] concludes that the error rate using traditional methods is approximately 50 %.

A bruise or skin hematoma is caused by blunt force to the skin, resulting in bleeding from capillaries. The vessels may continue to bleed some time after the impact, and the bruise develops during the first 24 – 48 hours [77]. The immediate tissue response to traumatic injury involves an acute inflammatory reaction initiated by the trauma. This reaction causes recruitment of neutrophils and macrophages from the vascular system [82, 83]. Macrophages and neutrophils engulf both erythrocytes and free hemoglobin molecules and initiate the heme oxygenase system to break down the hemoglobin and produce bilirubin and hemosiderin [42, 48]. Production of bilirubin causes bruises to appear yellow [45, 77].

The description of color development in bruised areas differs considerably. As an example, Langlois and Gresham [77] state that yellow color can be observed after 18 hours, while Schwartz and Ricci [79] state that yellow color has been reported between 7 days and 2 weeks after injury. The individual ability to perceive yellow color declines with age [84], and might introduce further individual differences to visual age determination.

The need for an objective, easy manageable method to date bruises is obvious. Reflectance spectroscopy has proved to be effective to monitor various skin conditions [1, 10, 38, 85, 86], and in this part of the thesis the applicability of reflectance spectroscopy to the characterization of bruises is investigated.

5.3.1   Paper V: Optical characterization of bruises

L.L. Randeberg, A. Winnem, S. Blindheim, O.A. Haugen, L.O. Svaasand, Optical classification of

bruises, Proceedings of SPIE, 5312:54 – 64, 2004

In this study reflectance spectroscopy was combined with the two layer diffusion model for light propagation to analyze the time development of sports injuries affecting the skin in otherwise healthy subjects. The purpose of this study was to identify possible markers for age determination of bruises, and to follow their development with time. Special attention was payed to the bilirubin content and oxygenation of the bruises.

In forensic science it is important to be able to quantify the bruising process and the time after injury, for use in *e. g.* police investigations. The need for an objective method to date contusions is obvious, and since a bruise goes through several clearly visible color changes, optical techniques would be a first choice. The size and development of a hematoma is determined by several factors, *e. g.* the impact causing the injury, body site, gender, age and skin thickness. Hemoglobin breakdown causes the visible color changes that can be observed in bruised skin as a function of time after injury.

This study presents reflectance spectra collected from bruises in otherwise healthy subjects. A total of 73 spectra of 25 bruises were measured on 13 individuals in the 400 – 850 nm wavelength region. All injuries were caused by sports activities such as judo and soccer. The bruises were classified according to visual appearance, bilirubin content, oxygenation, and age of injury. Only bruises with known age and cause were included in the study. Spectral changes of each hematoma were recorded over several days. Preliminary results show large variation in the spectra, caused by differences in age and depth of the bruises. The present data suggested that measurements of blood oxygenation, dermal blood volume fraction, and bilirubin level can be used to determine the age of contusions. Such an objective method to determine the age of an injury would be highly valuable in forensic medicine.

This paper was the very first approach from our group to do optical characterization of bruised skin. In this work bilirubin was focused on as the most important chromophore, although blood volume and blood oxygenation are also suggested as possible optical markers. This work was preliminary, and our experience with bruised skin was limited. Fortunately, the methods developed for port-wine stains proved to be useful also for bruised skin. Port-wine stains and especially purpura have reflectance characteristics resembling bruised skin. During the work with this paper we recognized the need for a larger study and a mathematical model to describe the physical processes occurring after a traumatic incidence.

5.3.2   Paper IX: Blood distribution in skin hematomas

L.L. Randeberg, O.A. Haugen, R. Haaverstad, L.O. Svaasand, Age determination of traumatic injuries, submitted to Lasers Surg Med, March 2005

This paper considers a mathematical method to describe the blood distribution in bruised tissue as a function of time after impact. The purpose of this study was to develop a reliable analytical model, and to validate this model against experimental data.

Bohnert et al. [87] used reflectance spectroscopy to study the depth and color of contusions post mortem, and found that shallow fresh bruises appear bright red, while deeper injuries show a more bluish color. Reflectance spectroscopy of bruises *in vivo* has been carried out with promising results [11, 88]. To further enhance the value of reflectance spectroscopy, the physics behind the changing skin appearance must be considered. To construct a physical model, the development of a bruise must be described mathematically. A trauma causing localized vessel damage may rapidly result in a pool of blood in subcutaneous tissues, which subsequently is transported deeper

into tissue. Hemoglobin will be transported into dermis by diffusion of whole and hemolyzed blood from the subcutaneous layer. These processes can be modelled analytically by the use of Darcy's law and diffusion theory.

To verify the theoretical model, data from skin hematomas in cardiothoracic patients were used. Reflectance spectra in the $400 - 850$ nm wavelength range were collected from normal and bruised skin using an integrating sphere setup. The subjects were adult patients admitted to the Department of cardiothoracic surgery, St. Olav's Hospital, Trondheim. The skin hematomas were caused by external trauma, cardiothoracic examinations or surgery. Special attention was payed to the dermal blood volume fraction and the hemoglobin oxygenation in bruised areas. Experimental evidence of a white central zone developing in injured areas were presented with a theory of its development.

Preliminary results show that measured and simulated skin reflectance agrees well, especially considering the multiple approximations applied within the model. The discrepancy that can be observed in simulated and measured spectra for wavelengths above approximately 650 nm is thought to be due to an artifact in the measurements. Red light penetrates deeper into tissue than other visible wavelengths and are therefore more readily scattered out of the collection angle of the integrating sphere.

The implemented model predicts the age of a hematoma with an accuracy of approximately 1 day. The accuracy of the method depends on precise information of skin thickness in the injured area. The quality of the estimates from the model will thus be enhanced if a reliable measure of skin thickness is collected concurrent with the reflection measurement. In conclusion the implemented model describes the time development of a skin hematoma with good accuracy. The analytic method provides a theoretical basis for developing a device to determine the age of injuries in forensic medicine.

This paper was the last paper written for this thesis. The original idea was to publish the model and the experimental evidence in two different papers. However, due to the limited time available due to patent issues, it was decided to go for an "all in one" publication. A larger study on the mechanical properties of skin and the relation between bruising and impact is planned, and will be initiated during 2005. Further patient studies are also planned to assure statistical significance.

Chapter 6

Conclusions and further work

"A conclusion is the place where you got tired of thinking."

Arthur Bloch

THIS thesis covers a wide field of applications, with emphasis on applications of reflectance spectroscopy for diagnostic purposes. Reflectance spectroscopy in the visible part of the spectrum has been proved to be a valuable tool in a variety of applications including *e. g.* port-wine stain diagnostics, diagnostics of liver pathology, neonatal jaundice and age determination of bruises for forensic applications.

Reflectance spectroscopy was found suitable to identify methemoglobin formation *in vivo* following laser exposure. Results presented in this thesis indicate that thermally induced methemoglobin formation is dose dependent *i. e.* temperature dependent. These findings may in the future lead to a greater understanding of the relationship between light doses and therapeutic outcome.

Reflectance spectroscopy was also found useful to detect age related chromophore changes in bruised skin. A mathematical method was developed to describe the temporal development of a bruise. A mathematical description of hemoglobin diffusion in skin was developed and combined with an existing method for photon transport. This new method is a first approach to mathematically describe temporal chromophore changes in bruised skin. Preliminary testing against experimental data, showed good correlation between the simulated age and the actual age of bruises. The age of a bruise could be determined with an accuracy of approximately 1 day. Further work is needed to test the algorithm on a larger selection of bruises.

Further work

Several of the studies included in this thesis are candidates for further work. Emphasis will be put on follow up studies of papers VI and IX. A study where laser treated patients are followed over time is required to establish the connection between light dose, methemoglobin formation and clinical response.

Forensic applications of reflectance spectroscopy have triggered a new area of focus. A larger study is planned to consider the relation between mechanical impact and bruising. Experiments

including biopsies will be carried out to investigate local changes within a bruised area. This is a interdisciplinary project which requires close collaboration between disciplines like mechanical engineering, electrical engineering, optics and medicine. New contacts have been established to explore the possibilities for hyper-spectral imaging of bruised tissue. Additional information about the spatial distribution of the chromophores within a bruise is of great interest. The commercial possibilities of the invented method will be considered in cooperation with the technology transfer office at the university.

Bibliography

[1] L. O. Svaasand, L. T. Norvang, E. J. Fiskerstrand, et al. Tissue parameters determining the visual appearance of normal skin and port wine stains. *Lasers Med Sci*, 10:55–65, 1995.

[2] V. K. Bhutani, G. R. Gourley, S. Adler, B. Kreamer, C. Dalin, and L. H. Johnson. Noninvasive measurement of total serum bilirubin in a multiracial predischarge newborn population to assess the risk of severe hyperbilirubinemia. *Pediatrics*, 106(2):(E17), 2000.

[3] K. M. Kelly and J. S. Nelson. Update on the clinical management of port wine stains. *Lasers Med Sci*, 15:220–226, 2000.

[4] S. Michel, M. Landthaler, and U. Hohenleutner. Recurrence of port-wine stains after treatment with the flashlamp-pumped pulsed dye laser. *Br J Dermatol*, 143:1230–1234, 2000.

[5] J. S. Nelson, T. E. Milner, B. Anvari, B. S. Tanenbaum, S. Kimel, L. O. Svaasand, and S. L. Jacques. Dynamic epidermal cooling during pulsed laser treatment of port-wine stain. A new methodology with preliminary clinical evaluation. *Arch Dermatol*, 131:695–700, 1995.

[6] J. K. Barton, G. Frangineas, H. Plummer, and J. F. Black. Cooperative phenomena in two-pulse, two-color laser photocoagulation of cutaneous blood vessels. *Photochem Photobiol*, 73(6):642–650, 2001.

[7] W. Verkruysse, A. M. K. Nilsson, T. E. Milner, J. F. Beek, G. W. Lucassen, and M. J. C. van Gemert. Optical absorption of blood depends on temperature during a 0.5 ms laser pulse at 586 nm. *Photochem Photobiol*, 67:276–281, 1998.

[8] N. Kollias, A. Baqer, I. Sadiq, and R. M. Sayre. *In vitro* and *in vivo* ultraviolet-induced alterations of oxy- and deoxyhemoglobin. *Photochem Photobiol*, 56(2):223–227, 1992.

[9] R. E. Schumacher. Noninvasive measurements of bilirubin in the newborn. *Clin Perinatol*, 17:417–435, 1990.

[10] Y. Yamauchi and J. Yamanouchi. Transcutaneous bilirubinometry: Bilirubin kinetics of the skin and serum during and after phototherapy. *Biol Neonate*, 56:263–269, 1989.

[11] V. K. Hughes, P. S. Ellis, T. Burt, and N. E. Langlois. The practical application of reflectance spectrophotometry for the demonstration of haemoglobin and its degradation in bruises. *J Clin Pathol*, 57(4):355–359, 2004.

[12] S. W. Jacob, C. A. Francone, and W. J. Lossow. *Anatomi og fysiologi*. Universitetsforlaget AS, 1985. Til norsk ved: E Dietrichs og P Hurlen.

[13] Encyclopaedia Britannica Online. Skin. `http://www.eb.com:180/bol/topic?eu=109297\&sctn=1`. Accessed April 2005.

[14] N. Agar and A. R. Young. Melanogenesis: A photoprotective response to DNA damage? *Mutat Res*, 571:121–132, 2004.

[15] R. R. Anderson and J. A. Parrish. The optics of human skin. *J Invest Dermatol*, 77(1):13–19, 1981.

[16] T. B. Fitzpatrick. The validity and practicality of sun-reactive skin types I through VI. *Arch Dermatol*, 124(6):869–871, 1998.

[17] Y. Ou-Yang, G. Stamatas, and N. Kollias. Spectral responses of melanin to ultraviolet A irradiation. *J Invest Dermatol*, 122:492–496, 2004.

[18] N. Kollias and A. H. Baqer. Absorption mechanisms of human melanin in the visible, 400–720 nm. *J Invest Dermatol*, 89(4):384–388, 1987.

[19] J. Sandby-Møller, T. Poulsen, and H. C. Wulf. Epidermal thickness at different body sites: Relationship to age, gender, pigmentation, blood content, skin type and smoking habits. *Acta Derm Venerol*, 83:410–413, 2003.

[20] A. Ishimaru. *Wave Propagation and Scattering in Random Media*, volume 1. Academic Press, New York, 1978.

[21] M. J. C. van Gemert, S. L. Jaques, H. J. C. M. Sterenborg, and W. M. Star. Skin optics. *IEEE Trans Biomed Eng*, 36:1146–1154, 1989.

[22] I. S. Saidi, S. L. Jaques, and F. K. Tittel. Mie and Rayleigh modeling of visible-light scattering in neonatal skin. *Appl Opt*, 34(31):7410–7418, 1995.

[23] M. L. Wolbarsht, A. W. Walsh, and G. George. Melanin, a unique biological absorber. *Appl Opt*, 20:2184–2186, 1981.

[24] J. M. Steinke and A. P. Shepard. Comparision of Mie theory and the light scattering of red blood cells. *Appl Opt*, 27:4027–4033, Oct 1988.

[25] W. G. Zijlstra, A. Buursma, and O. W. van Assendelft. *Visible and near infrared absorption spectra of human and animal haemoglobin*. VSP, Utrecht, 2000.

[26] H. Du, R. A. Fuh, J. Li, A. Corkan, and J. S. Lindsey. PhotochemCAD: A computer-aided design and research tool in photochemistry. *Photochem Photobiol*, 68:141–142, 1998.

[27] D. J. Weatherall, J. G. G. Ledningham, and D. A. Warrell, editors. *Oxford Textbook of Medicine*, chapter 19. Oxford University Press, 1983.

[28] D. B. Marks, A. D. Marks, and C. M. Smith. *Basic Medical Biochemistry*. Williams and Wilkins, Baltimore, 1996.

[29] V. Y. Baranov, D. I. Chekhov, A. G. Leonov, et al. Heat-induced changes in optical properties of human blood *in vitro*. *Proceedings of SPIE*, 3599:180–187, 1999.

[30] G. G. P. Fechner and D. J. Gee. Study on the effects of heat on blood and on the post-mortem estimation of carboxyhaemoglobin and methaemoglobin. *Forensic Sci Int*, 40:63–67, 1998.

[31] K. Farahani, R. E. Saxton, H-C. Yoon, A. A. F. de Salles, et al. MRI of thermally denatured blood: Methemoglobin formation and relaxation effects. *Magn Reson Imaging*, 17(10): 1489–1494, 1999.

[32] L. L Randeberg, A. J. Daae Hagen, and L. O. Svaasand. Optical properties of human blood as a function of temperature. *Proceedings of SPIE*, 4609:20–29, 2002.

[33] L. L. Randeberg, J. H. Bonesrønning, M. Dalaker, J. S. Nelson, and L. O. Svaasand. Methemoglobin formation during laser induced photothermolysis of skin vascular lesions. *Lasers Surg Med*, 34(5):414–419, 2004.

[34] J. M. Steinke and A. P. Shepard. Diffusion model of the optical absorbance of whole blood. *J Opt Soc Am*, 5(6):813–822, 1988.

[35] C. L. Thomas, editor. *Taber's cyclopedic medical dictionary*. F. A. Davis Company, Philadelphia, 17th edition, 1993.

[36] W. E. Nelson. *Textbook of Pediatrics*. W B saunders Company, 15th edition, 1996.

[37] R. Graaff, J. G. Aarnoudse, J. R. Zijp, et al. Reduced light-scattering properties for mixtures of spherical particles: A simple approximation derived from Mie calculations. *Appl Opt*, 31: 1370–1376, Apr 1992.

[38] T. Spott, L. O. Svaasand, R. E. Anderson, and P. F. Schmedling. Application of optical diffusion theory to transcutaneous bilirubinometry. *SPIE Europto Series*, 3195:234–245, 1997.

[39] L. L. Randeberg, E. B. Roll, L. T. Norvang Nilsen, T. Christensen, and L. O. Svaasand. *In vivo* spectroscopy of newborn skin reveals more than a bilirubin index. *Acta Paediatr*, 94(1): 65–71, 2005.

[40] T. Spott. *Characterization of layered tissue structures with diffusely propagating photon density waves*. Doctoral thesis, Norwegian University of Science and Technology, Trondheim, Norway, 1999. Fys. El. rapport 1999:50.

[41] A. F. McDonagh and D. A. Lightner. 'Like a Shrivelled Blood Orange' – Bilirubin, jaundice, and phototherapy. *Pediatrics*, 75(3), Mar 1985.

[42] D. Gemsa and R. Schmid. Hämoglobinstoffwechsel und bilirubinbildung. *Klin Wschr*, 52: 609–616, 1974.

[43] R. Tenhunen, H. S. Marver, and R. Schmid. Microsomal heme oxygenase: Characterisation of the enzyme. *J Biol Chem*, 244(23):6388–6394, 1969.

[44] R. Wennberg. Bilirubin transport and toxicity. *Mead Johnson Symp Perinat Dev Med*, 19: 25–31, 1982.

[45] R. Virchow. Die pathologischen pigments. *Arch Pathol Anat*, 1:379–486, 1847.

[46] F. A. Wagener, H. D. Volk, D. Willis, N. G. Abraham, M. P. Soares, G. J. Adema, and C. G. Figdor. Different faces of the heme-heme oxygenase system in inflammation. *Harmacol Rev*, 55(3):551–571, 2003.

[47] M. D. Maines and J. Cohn. Bile pigment formation by skin heme oxygenase: Studies on the response of the enzyme to heme compounds and tissue injury. *J Exp Med*, 145(4):1054–1059, 1977.

[48] N. R. Pimstone, R. Tenhunen, P. T. Seitz, H. S. Marver, and R. Schmid. The enzymatic degradation of hemoglobin to bile pigments by macrophages. *J Exp Med*, 133(6):1264–1281, 1971.

[49] K. Laiho and R. Tenhunen. Hemoglobin degrading enzymes in experimental subcutaneous hematomas. *Z Rechtsmed*, 93:193–198, 1984.

[50] CambridgeSoft. ChemACX. `http://chemacx.cambridgesoft.com/`. Accessed April 2005.

[51] S. Wan, R. R. Anderson, and J. A. Parrish. Analytical modeling for the optical properties of the skin *in vitro* and *in vivo* applications. *Photochem Photobiol*, 34:493–499, 1981.

[52] J. D. Reagan and Parrish J. A., editors. *The Science of Photomedicine*, chapter "Optical properties of human skin". Plenum Press, New York, 1982.

[53] F. A. Duck. *Physical Properties of Tissue*. Academic Press, London, 1990.

[54] W. Stahl, U. Heinrich, H. Jungmann, J. von Laar, M. Schietzel, H. Sies, and H. Tronnier. Increased dermal carotenoid levels assessed by noninvasive reflection spectrophotometry correlate with serum levels in women ingesting betatene. *J Nutr*, 128:903–907, 1998.

[55] G. E. Piérard. EEMCO guidance for the assessment of skin colour. *J Eur Acad Dermatol Venereol*, 10:1–11, 1998.

[56] H. K. Biesalski and U. C. Obermueller-Jevic. UV light, beta-carotene and human skin – Beneficial and potentially harmful effects. *Arch Biochem Biophys*, 389(1):1–6, 2001.

[57] R. M. Pope and E. S. Fry. Absorption spectrum (380–700 nm) of pure water. II. Integrating cavity measurements. *Appl Opt*, 36:8710–8723, 1997.

[58] Standard CIE 15.2:1986. *Colorimetry*. Commision Internationale L'Éclairage, 2nd edition, 1986.

[59] V. R. Weidner and J. J. Hsia. Reflection properties of pressed polytetrafluoroethylene powder. *J Opt Soc Am A*, 71:856–861, 1981.

[60] L. T. Norvang. *In Vivo Spectroscopy of Human Skin; Characterisation of Port Wine Stain*. PhD thesis, Norwegian University of Technology and Science (NTNU), Trondheim, Norway, Nov 1996.

[61] R. C. Haskell, L. O. Svaasand, T-T. Tsay, et al. Boundary conditions for the diffusion equation in radiative transfer. *J Opt Soc Am A*, 11:2727–2741, Oct 1994.

[62] T. Spott and L. O. Svaasand. Collimated light sources in the diffusion approximation. *Appl Opt*, 39(34):6453–6465, 2000.

[63] L. T. Norvang, E. J. Fiskerstrand, K. König, et al. Comparision between reflectance spectra obtained with an integrating sphere and a fiber-optic collection system. *SPIE Europto Series*, 2624:155–64, 1995.

[64] K. D. Jürgens, T. Peters, and G. Gros. Diffusion of myoglobin in intact skeletal muscle cells. *Proc Natl Acad Sci*, 9:3829–3833, 1994.

[65] A. Troilius, B. Wrangsjö, and B. Ljunggren. Patients with port wine stains and their psychosocial reactions after photothermolytic treatment. *Dermatol Surg*, 26(3):190–196, 2000.

[66] E. J. Fiskerstrand, L. O. Svaasand, G. Kopstad, M. Dalaker, L. T. Norvang, and G. Volden. Laser treatment of port-wine stains: Therapeutic outcome in relation to morphological parameters. *Br J Dermatol*, 134:1039–1043, 1996.

[67] S. S. Orten, M. Waner, S. Flock, P. K. Robertson, and J. Kincannon. Port-wine stains, an assessment of 5 years of treatment. *Arch Otolaryngol Head Neck Surg*, 122:1174–1179, 1996.

[68] Standard IEC 61966-2.1:1999. *Colour Measurement and Management in Multimedia Systems and Equipment. Part 2.1: Default RGB Colour Space - sRGB*. International Electrotechnical Organization.

[69] J. Gondek. An extended sRGB space for high quality consumer imaging. `http://w3.hike.te.chiba-u.ac.jp/IEC/100/PT61966/parts/part2/`. Accessed Jun 2000.

[70] S. Mordon, D. Brisot, and N. Fournier. Using a non uniform pulse sequence can improve selective coagulation with a Nd:YAG laser (1.06 μm) thanks to met-hemoglobin absorption: A clinical study on blue leg veins. *Lasers Surg Med*, 32(2):160–170, 2003.

[71] E. V. Ross and Y. Domankevitz. Laser treatment of leg veins: Physical mechanisms and theoretical considerations. *Lasers Surg Med*, 36(2):105–116, 2005.

[72] B. M. Pikkula, D. W. Chang, J. S. Nelson, and B. Anvari. Comparison of 585 and 595 nm laser-induced vascular response of normal in vivo human skin. *Lasers Surg Med*, 36(2):117–123, 2005.

[73] T. H. Dai, B. M. Pikkula, L. V. Wang, and others. Comparison of human skin opto-thermal response to near-infrared and visible laser irradiations: A theoretical investigation. *Phys Med Biol*, 49(21):4861–4877, 2004.

[74] J. F. Black, N. Wade, and J. K. Barton. Mechanistic comparison of blood undergoing laser photocoagulation at 532 and 1,064 nm. *Lasers Surg Med*, 36(2):155–165, 2005.

[75] S. Sherlock and J. Dooley. *Diseases of the liver and biliary system*, chapter 23: "Nutritional and Metabolic Liver Diseases". Blackwell Science, Oxford, 10th edition, 1997.

[76] R. Rubin and J. L. Farber, editors. *Pathology*, chapter "The liver and biliary system". Lipincott-Raven, Philadelphia, 3rd edition, 1999.

[77] N. E. I. Langlois and G. A. Gresham. The aging of bruises; A review and study of the colour changes with time. *Forensic Sci Int*, 50:227–238, 1991.

[78] T. Stephenson and Y. Bialas. Estimation of the age of bruising. *Arch Dis Child*, 74(1):53–55, 1996.

[79] A. J. Schwartz and L. R. Ricci. How accurately can bruises be aged in abused children? Literature review and synthesis. *Pediatrics*, 97(2):254–257, 1996.

[80] W. A. Altemeier. Interpreting bruises in children. *Pediatr Ann*, 30(9):517–520, 2001.

[81] S. Maguire, M. K. Mann, J. Sibert, and A. Kemp. Can you age bruises accurately in children? A systematic review. *Arch Dis Child*, 90:187–189, 2005.

[82] D. A. Hume, I. L. Ross, R. Himes, R. T. Sasmono, C. A. Wells, and T. Ravasi. The mononuclear phagocyte system revisited. *J Leukoc Biol*, 72:621–627, 2002.

[83] R. N. Thornton and R. D. Jolly. The objective interpretation of histopathological data: An application to the aging of ovine bruises. *Forensic Sci Int*, 31:225–239, 1986.

[84] V. K. Hughes, P. S. Ellis, and N. E. Langlois. The perception of yellow in bruises. *J Clin Forensic Med*, 11(5):257–259, 2004.

[85] D. I. Tudehope and A. Chang. Multiple site readings from a transcutaneous bilirubinometer. *Aust Paediatr J*, 18:102–105, 1982.

[86] L. T. Norvang, T. E. Milner, J. S. Nelson, M. W. Berns, and L. O. Svaasand. Skin pigmentation characterized by visible reflectance measurements. *Lasers Med Sci*, 12:99–112, 1997.

[87] M. Bohnert, R. Baumgartner, and S. Pollak. Spectrophotometric evaluation of the colour of intra and subcutaneous bruises. *Int J Legal Med*, 113:343–348, 2000.

[88] L. L Randeberg, A. M. Winnem, S. Blindheim, O. A. Haugen, and L. O. Svaasand. Optical classification of bruises. *Proceedings of SPIE*, 5312:54–64, 2004.